www.sciencemag.org/content/362/6418/1031/suppl/DC1

Supplementary Materials for

A gamma-ray determination of the Universe's star formation history

The Fermi-LAT Collaboration*

*Email: majello@g.clemson.edu; helgason@hi.is; vpaliya@g.clemson.edu; justin.finke@nrl.navy.mil; abhishd@g.clemson.edu; alberto@gae.ucm.es

Published 30 November 2018, *Science* **362**, 1031 (2018)
DOI: 10.1126/science.aat8123

This PDF file includes:

Other supplementary material for this manuscript includes the following:

Data S1 (machine-readable version of table S4; .txt file)

Authors and Affiliations

S. Abdollahi[1], M. Ackermann[2], M. Ajello[3]†, W. B. Atwood[4], L. Baldini[5], J. Ballet[6], G. Barbiellini[7,8], D. Bastieri[9,10], J. Becerra Gonzalez[11,12], R. Bellazzini[13], E. Bissaldi[14,15], R. D. Blandford[16], E. D. Bloom[16], R. Bonino[17,18], E. Bottacini[16,19], S. Buson[11], J. Bregeon[20], P. Bruel[21], R. Buehler[2], R. A. Cameron[16], R. Caputo[22], P. A. Caraveo[23], E. Cavazzuti[24], E. Charles[16], S. Chen[9,19], C. C. Cheung[25], G. Chiaro[23], S. Ciprini[26,27], J. Cohen-Tanugi[20], L. R. Cominsky[28], J. Conrad[29,30], D. Costantin[10], S. Cutini[26,27], F. D'Ammando[31,32], F. de Palma[15,33], A. Desai[3]†, S. W. Digel[16], N. Di Lalla[5], M. Di Mauro[16], L. Di Venere[14,15], A. Domínguez[34]†, C. Favuzzi[14,15], S. J. Fegan[21], J. Finke[25]†, A. Franckowiak[2], Y. Fukazawa[1], S. Funk[35], P. Fusco[14,15], G. Gallardo Romero[2,36], F. Gargano[15], D. Gasparrini[26,27], N. Giglietto[14,15], F. Giordano[14,15], M. Giroletti[31], D. Green[12,11], I. A. Grenier[6], L. Guillemot[37,38], S. Guiriec[39,11], D. H. Hartmann[3], E. Hays[11], K. Helgason[40,42]†, D. Horan[21], G. Jóhannesson[41,42], D. Kocevski[11], M. Kuss[13], S. Larsson[43,30], L. Latronico[17], J. Li[2], F. Longo[7,8], F. Loparco[14,15], B. Lott[44], M. N. Lovellette[25], P. Lubrano[27], G. M. Madejski[16], J. D. Magill[12], S. Maldera[17], A. Manfreda[5], L. Marcotulli[3], M. N. Mazziotta[15], J. E. McEnery[11,12], M. Meyer[16], P. F. Michelson[16], T. Mizuno[45], M. E. Monzani[16], A. Morselli[46], I. V. Moskalenko[16], M. Negro[17,18], E. Nuss[20], R. Ojha[11], N. Omodei[16], M. Orienti[31], E. Orlando[16], J. F. Ormes[47], M. Palatiello[7,8], V. S. Paliya[3]†, D. Paneque[48], J. S. Perkins[11], M. Persic[7,49], M. Pesce-Rollins[13], V. Petrosian[16], F. Piron[20], T. A. Porter[16], J. R. Primack[4], G. Principe[35], S. Rainò[14,15], R. Rando[9,10], M. Razzano[13,51], S. Razzaque[50], A. Reimer[51,16], O. Reimer[51,16], P. M. Saz Parkinson[4,52,53], C. Sgrò[13], E. J. Siskind[54], G. Spandre[13], P. Spinelli[14,15], D. J. Suson[55], H. Tajima[56,16], M. Takahashi[48], J. B. Thayer[16], L. Tibaldo[57,58], D. F. Torres[59,60], E. Torresi[61], G. Tosti[27,62], A. Tramacere[63], E. Troja[11,12], J. Valverde[21], G. Vianello[16], M. Vogel[64], K. Wood[65], G. Zaharijas[66,67]

1. Department of Physical Sciences, Hiroshima University, Higashi-Hiroshima, Hiroshima 739-8526, Japan

2. Deutsches Elektronen Synchrotron DESY, D-15738 Zeuthen, Germany

3. Department of Physics and Astronomy, Clemson University, Kinard Lab of Physics, Clemson, SC 29634-0978, USA

4. Santa Cruz Institute for Particle Physics, Department of Physics and Department of Astronomy and Astrophysics, University of California at Santa Cruz, Santa Cruz, CA 95064, USA

5. Università di Pisa and Istituto Nazionale di Fisica Nucleare, Sezione di Pisa I-56127 Pisa, Italy

6. Laboratoire Astrophysique Interactions Multi-échelles, Commissariat á l'énergie atomique-Institute of Research into the Fundamental Laws of the Universe/Centre national de la recherche scientifique/Université Paris Diderot, Service d'Astrophysique, Commissariat á l'énergie atomique Saclay, F-91191 Gif sur Yvette, France

7. Istituto Nazionale di Fisica Nucleare, Sezione di Trieste, I-34127 Trieste, Italy

8. Dipartimento di Fisica, Università di Trieste, I-34127 Trieste, Italy

9. Istituto Nazionale di Fisica Nucleare, Sezione di Padova, I-35131 Padova, Italy

10. Dipartimento di Fisica e Astronomia "G. Galilei", Università di Padova, I-35131 Padova, Italy

11. National Aeronautics and Space Administration Goddard Space Flight Center, Greenbelt, MD 20771, USA

12. Department of Astronomy, University of Maryland, College Park, MD 20742, USA

13. Istituto Nazionale di Fisica Nucleare, Sezione di Pisa, I-56127 Pisa, Italy

14. Dipartimento di Fisica "M. Merlin" dell'Università e del Politecnico di Bari, I-70126 Bari, Italy

15. Istituto Nazionale di Fisica Nucleare, Sezione di Bari, I-70126 Bari, Italy

16. W. W. Hansen Experimental Physics Laboratory, Kavli Institute for Particle Astrophysics and Cosmology, Department of Physics and SLAC National Accelerator Laboratory, Stanford University, Stanford, CA 94305, USA

17. Istituto Nazionale di Fisica Nucleare, Sezione di Torino, I-10125 Torino, Italy

18. Dipartimento di Fisica, Università degli Studi di Torino, I-10125 Torino, Italy

19. Department of Physics and Astronomy, University of Padova, Vicolo Osservatorio 3, I-35122 Padova, Italy

20. Laboratoire Univers et Particules de Montpellier, Université Montpellier, Centre national de la recherche scientifique/Institut national de physique nucléaire de physique des particules, F-34095 Montpellier, France

21. Laboratoire Leprince-Ringuet, École polytechnique, Centre national de la recherche scientifique/Institut national de physique nucléaire de physique des particules, F-91128 Palaiseau, France

22. Center for Research and Exploration in Space Science and Technology (CRESST) and National Aeronautics and Space Administration Goddard Space Flight Center, Greenbelt, MD 20771, USA

23. Istituto Nazionale di Astrofisica-Istituto di Astrofisica Spaziale e Fisica Cosmica Milano, via E. Bassini 15, I-20133 Milano, Italy

24. Italian Space Agency, Via del Politecnico snc, 00133 Roma, Italy

25. Space Science Division, Naval Research Laboratory, Washington, DC 20375-5352, USA

26. Space Science Data Center - Agenzia Spaziale Italiana, Via del Politecnico, snc, I-00133, Roma, Italy

27. Istituto Nazionale di Fisica Nucleare, Sezione di Perugia, I-06123 Perugia, Italy

28. Department of Physics and Astronomy, Sonoma State University, Rohnert Park, CA 94928-3609, USA

29. Department of Physics, Stockholm University, AlbaNova, SE-106 91 Stockholm, Sweden

30. The Oskar Klein Centre for Cosmoparticle Physics, AlbaNova, SE-106 91 Stockholm, Sweden

31. Istituto Nazionale di Astrofisica Istituto di Radioastronomia, I-40129 Bologna, Italy

32. Dipartimento di Astronomia, Università di Bologna, I-40127 Bologna, Italy

33. Università Telematica Pegaso, Piazza Trieste e Trento, 48, I-80132 Napoli, Italy

34. Grupo de Altas Energías, Universidad Complutense de Madrid, E-28040 Madrid, Spain

35. Friedrich-Alexander-Universität Erlangen-Nürnberg, Erlangen Centre for Astroparticle Physics, Erwin-Rommel-Str. 1, 91058 Erlangen, Germany

36. Circolo Astrofili Talmassons, I-33030 Campoformido (UD), Italy

37. Laboratoire de Physique et Chimie de l'Environnement et de l'Espace – Université d'Orléans / Centre national de la recherche scientifique, F-45071 Orléans Cedex 02, France

38. Station de radioastronomie de Nançay, Observatoire de Paris, Centre national de la recherche scientifique/Institut national des sciences de l'univers, F-18330 Nançay, France

39. The George Washington University, Department of Physics, 725 21st St, NW, Washington, DC 20052, USA

40. Max-Planck-Institut für Astrophysik, Postfach 1317, D-85741 Garching, Germany

41. Science Institute, University of Iceland, IS-107 Reykjavik, Iceland

42. Kungliga Tekniska högskolan Royal Institute of Technology and Stockholm University, Roslagstullsbacken 23, SE-106 91 Stockholm, Sweden

43. Department of Physics, Kungliga Tekniska högskolan Royal Institute of Technology, AlbaNova, SE-106 91 Stockholm, Sweden

44. Centre d'Études Nucléaires de Bordeaux Gradignan, Institut national de physique nucléaire de physique des particules/Centre national de la recherche scientifique, Université Bordeaux 1, BP120, F-33175 Gradignan Cedex, France

45. Hiroshima Astrophysical Science Center, Hiroshima University, Higashi-Hiroshima, Hiroshima 739-8526, Japan

46. Istituto Nazionale di Fisica Nucleare, Sezione di Roma "Tor Vergata", I-00133 Roma, Italy

47. Department of Physics and Astronomy, University of Denver, Denver, CO 80208, USA

48. Max-Planck-Institut für Physik, D-80805 München, Germany

49. Osservatorio Astronomico di Trieste, Istituto Nazionale di Astrofisica, I-34143 Trieste, Italy

50. Department of Physics, University of Johannesburg, PO Box 524, Auckland Park 2006, South Africa

51. Institut für Astro- und Teilchenphysik and Institut für Theoretische Physik, Leopold-Franzens-Universität Innsbruck, A-6020 Innsbruck, Austria

52. Department of Physics, The University of Hong Kong, Pokfulam Road, Hong Kong, China

53. Laboratory for Space Research, The University of Hong Kong, Hong Kong, China

54. Nycb Real-Time Computing Inc., Lattingtown, NY 11560-1025, USA

55. Purdue University Northwest, Hammond, IN 46323, USA

56. Solar-Terrestrial Environment Laboratory, Nagoya University, Nagoya 464-8601, Japan

57. Centre national de la recherche scientifique, Institut de Recherche en Astrophysique et Planétologie, F-31028 Toulouse cedex 4, France

58. Galaxies Astrophysique des Hautes Énergies Cosmologie, Universit de Toulouse, Université Paul Sabatier-Observatoire midi-pyrénées, Institut de Recherche en astrophysique et planétologie, F-31400 Toulouse, France

59. Institute of Space Sciences (Consejo Superior de Investigaciones Cientficas-Institut d'Estudis Espacials de Catalunya), Campus Universitat Autónoma de Barcelona, Carrer de Magrans s/n, E-08193 Barcelona, Spain

60. Institució Catalana de Recerca i Estudis Avançats (ICREA), E-08010 Barcelona, Spain

61. Istituto Nazionale di Fisica Nucleare-Istituto di Astrofisica Spaziale e Fisica Cosmica Bologna, via P. Gobetti 101, I-40129 Bologna, Italy

62. Dipartimento di Fisica, Università degli Studi di Perugia, I-06123 Perugia, Italy

63. INTErnational Gamma-Ray Astrophysics Laboratory Science Data Centre, CH-1290 Versoix, Switzerland

64. California State University, Los Angeles, Department of Physics and Astronomy, Los Angeles, CA 90032, USA

65. Praxis Inc., Alexandria, VA 22303, resident at Naval Research Laboratory, Washington, DC 20375, USA

66. Istituto Nazionale di Fisica Nucleare, Sezione di Trieste, and Università di Trieste, I-34127 Trieste, Italy

67. Center for Astrophysics and Cosmology, University of Nova Gorica, Nova Gorica, Slovenia

† majello@g.clemson.edu, helgason@hi.is, vpaliya@g.clemson.edu, justin.finke@nrl.navy.mil, abhishd@g.clemson.edu, alberto@gae.ucm.es

Materials and Methods

Sample Selection and Data Analysis

Our sample is selected starting from the objects reported in the third catalog of active galactic nuclei detected by the LAT, 3LAC, (*43*). We exclude all the blazars reported there with a double association and those lacking a redshift measurement. Most redshift measurements for BL Lacs reported in 3LAC come from (*44*). For each source we assess the significance of the detection (between 1 GeV and 1 TeV) defining a test statistics (TS) as $TS = 2\Delta \log \mathscr{L}$, where $\mathscr{L}$ represents the likelihood function between models with and without the source of interest. We use this to exclude all sources that have a $TS < 25$ in this analysis. Our final sample comprises 419 FSRQs and 320 BL Lacs distributed (see Figure S1) between a redshift of 0.03 and 3.1.

The analysis relies on 101 months (Aug. 2008 to Jan. 2017) of Pass 8 (P8) class 'SOURCE' photons detected by the LAT between 1 GeV and 1 TeV. This dataset was filtered to eliminate times when the spacecraft was over the South Atlantic Anomaly and to remove photons detected at angles larger than 100° from the zenith. For the analysis of each source we use photons within 15° of the source position (region of interest, ROI). For each ROI we define a sky model that comprises the diffuse Galactic (*45*) and extragalactic emission (*46*) as well as the emission

from background sources in the ROI. The latter includes sources detected in the third *Fermi*-LAT catalog, 3FGL, (*47*) as well as any new source that is detected because of the additional exposure (with respect to the 3FGL) used here. These sources are found generating a TS map and identified as excesses above a $TS = 25$ threshold and added to the sky model with a power-law spectrum. The LAT 'P8R2_SOURCE_V6' instrumental response function (IRF) and a binned likelihood method are used to fit the sky model to the data.

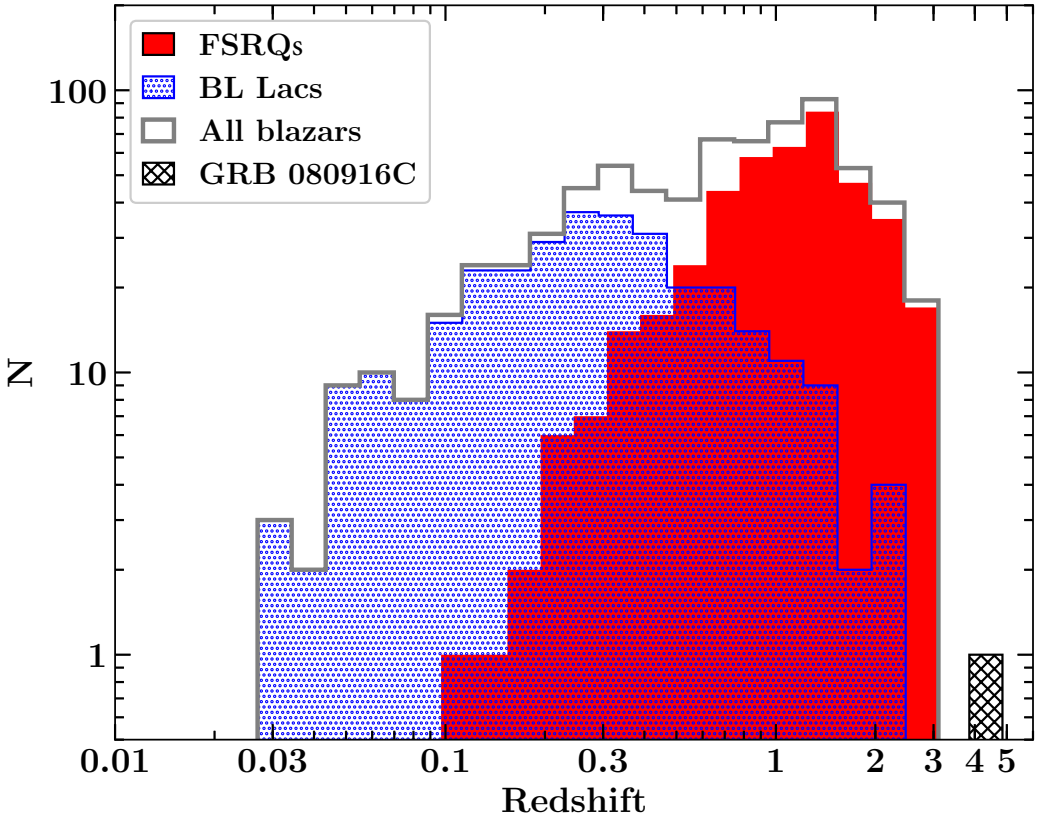

Figure S1 **Redshift distribution of the sources used in this analysis on a logarithmic scale.**

Intrinsic Spectra of Blazars

To capture the intrinsic curvature in the spectra of blazars we adopt the following strategy that has been optimized using simulations prior to the data analysis (see below). The data are fitted only to a maximum energy up to which the attenuation of the EBL is negligible. This is defined as the energy at which the optical depth $\tau_{\gamma\gamma}$<0.1 for the model of (*29*). However, we tested that our analysis is robust against changes of EBL model used to define this maximum energy and changes to the threshold (from e.g. $\tau_{\gamma\gamma} < 0.1$ to $\tau_{\gamma\gamma} < 0.05$). The optical depth decreases sharply

Table S1. Criteria, optimized on simulations, adopted to choose a spectral model.

$TS_{c,1}$	$TS_{c,2}$	Model Chosen
< 1	< 3	Log-parabola
> 1	< 3	Power law with exponential cut-off with γ_1=0.5
	> 3	Power law with exponential cut-off with γ_1 free

in this regime where not many EBL photons are expected due to a characteristic drop-off at the Lyman-limit (13.6 eV). Our baseline model for the intrinsic blazar spectrum is a log-parabola:

$$\frac{\mathrm{d}N}{\mathrm{d}E} = N_0 \left(\frac{E}{E_b}\right)^{-\alpha+\beta\log(E/E_b)} \tag{S1}$$

where N_0 (the normalization), α (photon index), β (curvature) are all free parameters and E_b is a scaling energy. We also test whether an exponential power law could be a better representation of the blazar spectrumand this is defined as:

$$\frac{\mathrm{d}N}{\mathrm{d}E} = N_0 \left(\frac{E}{E_c}\right)^{\alpha} e^{-(E/E_b)^{\gamma_1}} \tag{S2}$$

where E_c (cut off energy) and γ_1 (the exponential index) are all free parameters. Smoothed broken power laws and broken power laws were also tested, but they were never found to describe the blazar intrinsic spectrum better than the two models reported above in the energy range used in this work.

When testing the exponential cut-off model we perform a first fit with γ_1 fixed at 0.5 (justified from the observations of hundreds of FSRQs, see (*48*)) and then another fit leaving γ_1 free to vary. We define two TS of curvature $TS_{\mathrm{c,1}}$ and $TS_{\mathrm{c,2}}$ as follows:

$$TS_{\mathrm{c,1}} = 2(\log L_{\mathrm{exp},\gamma_1=0.5} - \log L_{\log-\mathrm{parabola}}) \tag{S3}$$

$$TS_{\mathrm{c,2}} = 2(\log L_{\mathrm{exp},\gamma_1=\mathrm{free}} - \log L_{\log-\mathrm{parabola}}). \tag{S4}$$

where $\log L_{\mathrm{exp},\gamma_1=0.5}$ and $\log L_{\mathrm{exp},\gamma_1=\mathrm{free}}$ are the log-likelihoods derived using the exponential cut-off model with $\gamma_1 = 0.5$ and γ_1 free to vary respectively and $\log L_{\log-\mathrm{parabola}}$ is the log-likelihood of the log-parabola model.

We adopt the criteria reported in Table S1 to choose the model used to describe each blazar's intrinsic spectrum. In order to avoid convergence problems, in the analysis presented above, the exponential index γ_1 remains fixed at either 0.5 or the best-fitting value found at this step. The median of the distribution of fitted γ_1 values is $\approx$0.5.

Analysis

Results for Blazars

Once the choice of the intrinsic spectrum for the sources has been made, the analysis reverts to using the full, 1 GeV–1 TeV, energy band and the modeled spectra of all sources include the EBL attenuation as reported in Equation 1, where b is a parameter, common to all sources, that is varied to fit the EBL model prediction to the data. A $b = 1$ would mean that the EBL model predictions are in agreement with the LAT data, while a $b = 0$ would imply that there is no evidence for attenuation due to absorption by EBL photons in the spectra of blazars.

Because of the complexity of the problem, the b parameter is not optimized in one stage. Instead, for each source we scan the likelihood function in very small steps of b creating a profile likelihood. In this process, the parameters of the diffuse emission, those of the brightest sources, and those of the source of interest (except γ_1) are all left free to vary. For each source, the best-fitting b value is the one that maximizes the log-likelihood. A TS of the detection of the EBL can be built comparing the log-likelihood values at the best-fitting $b = b_0$ and at $b = 0$ as $TS_{\rm EBL} = 2[\log L(b_0) - \log L(b = 0)]$. Because log-likelihoods (and thus TS) are additive, we can determine the b value that maximizes the global (for all sources) likelihood and produces the largest $TS_{\rm EBL}$. In Figure S2, we plot the TS profile, as a function of b, for all sources (and separately for BL Lacs and FSRQs) for the model of (*29*). A b=1.03 improves the fit by a TS of $\sim$300, which corresponds to $\sim 17\,\sigma$ for one degree of freedom. We note that the spectral evolution of the blazar class with redshift has a negligible effect on this analysis, as apparent from Figure S2, which shows that the level of EBL measured using (mostly) hard-spectrum BL Lacs is in very good agreement with that found using soft-spectrum FSRQs. As an additional test we report the values of the b parameter for the model of (*29*) for BL Lacs with a synchrotron peak frequency $> 10^{16}$ Hz (called HSPs) and for the remaining BL Lacs; these are respectively $b_{\rm HSPs} = 0.98^{+0.09}_{-0.13}$ ($TS_{\rm EBL}$=125.8) and $b_{\rm rest} = 0.86^{+0.16}_{-0.10}$ ($TS_{\rm EBL} = 45.1$). These highlight once more that there is no bias in the level of the EBL due to the spectral evolution of the blazar class.

One can also measure the compatibility of a model prediction with the *Fermi*-LAT data defining a TS as $TS_{b=1} = 2[\log L(b_0) - \log L(b = 1)]$. By definition a large $TS_{b=1}$ implies that the model predictions are in tension with the *Fermi*-LAT data; this typically happens when the model predicts a larger-than-observed attenuation. Table S2 shows the results of our analysis for some of the models available in the literature that have not been found in tension with previous γ-ray data. The table shows that the high model of (*49*) and the best-fitting model of (*50*) are excluded. Moreover, the models of (*51*) and (*37*) are found in tension at the $\sim 3\,\sigma$ level with the *Fermi*-LAT observations. All these models predict a larger optical-UV intensity of the EBL than the models compatible with the LAT data.

The optical depth as a function of energy and redshift can be measured by repeating the above procedure (i.e., renormalizing the optical depth predicted by a model), but in small energy and redshift bins. In this process, the uncertainty due to the small disagreement between different EBL models, about the shape of the optical depth curve within any given bin, has

Table S2. Joint-likelihood results for different EBL models (first and second columns) ordered by decreasing value of the last column. The third column refers to the significance, in units of σ, of the attenuation in the spectra of blazars when a given EBL model is scaled by the factor b. In this case b=0 (i.e., no EBL absorption) constitutes the null hypothesis. The fourth column lists the maximum likelihood values and 1 σ confidence ranges for the opacity scaling factor. In the last column, the b=1 case (i.e., EBL absorption as predicted by a given EBL model) constitutes the null hypothesis. This column shows the compatibility (expressed in units of σ) of the predictions of EBL models with the *Fermi*-LAT observations. Large values mean less likely to be compatible.

Model	Ref.	Significance of b=0 Rejection	b	Significance of b=1 Rejection
Scully et al. (2014) – high	(*49*)	16.0	0.42 ± 0.03	17.4
Kneiske et al. (2004) – best -fit	(*50*)	16.9	0.68 ± 0.05	6.0
Gilmore et al. (2012) – fixed	(*51*)	16.7	1.30 ± 0.10	3.0
Gilmore et al. (2012) – fiducial	(*51*)	16.6	0.81 ± 0.06	2.9
Dominguez et al. (2011)	(*37*)	16.6	1.31 ± 0.10	2.9
Franceschini et al. (2017)	(*52*)	16.4	1.25 ± 0.10	2.5
Gilmore et al. (2009)	(*53*)	16.7	1.03 ± 0.08	2.4
Inoue et al. (2013)	(*54*)	16.2	0.87 ± 0.06	2.1
Kneiske & Dole (2010)	(*55*)	16.8	0.94 ± 0.08	1.7
Helgason et al. (2012)	(*38*)	16.5	1.10 ± 0.08	1.3
Finke et al. (2010) – model C	(*29*)	17.1	1.03 ± 0.08	0.4
Scully et al. (2014) – low	(*49*)	16.0	1.00 ± 0.07	0.1

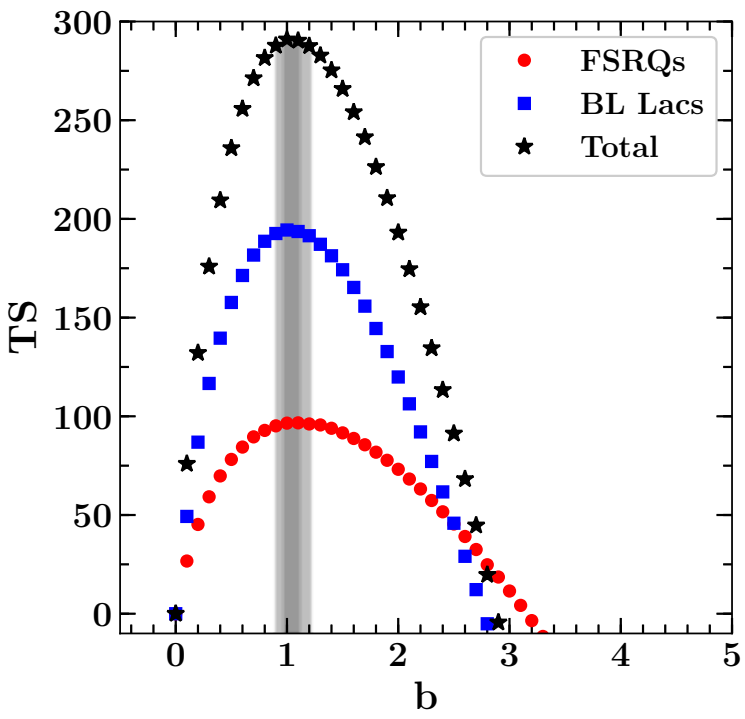

Figure S2 **Detection of the attenuation of the EBL.** Test statistics of the EBL as a function of the scaling parameter b adopting the model of (*29*). The shaded regions show the $1\,\sigma$ and $2\,\sigma$ confidence intervals around the best fitting value of b. This TS profile was obtained by summing the TS profiles of every source, including variable sources.

been included in the final uncertainty of the optical depth. The final uncertainty includes also the 10 % systematic uncertainty discussed below. The redshift bins were chosen so that similar values of $TS_{\rm EBL}$ were obtained in all the bins. Figure S3 shows measurements of the optical depth $\tau_{\gamma\gamma}$ due to EBL absorption in different redshift and energy bins. It is apparent from the figure that most of the constraining power is around $\tau_{\gamma\gamma} \approx 1$. Formally the $\tau_{\gamma\gamma}(E, z) = 1$ value marks the cosmic γ-ray horizon, i.e., the energy above which our Universe becomes opaque to γ rays for a given redshift (*56, 57*). The energy at which $\tau_{\gamma\gamma}(E, z) = 1$ at any redshift can be found by renormalizing any EBL model to fit the data presented in Figure S3 and propagating the (statistical plus systematic) uncertainties. Figure 1 shows that *Fermi* LAT maps the horizon position with energy from low ($z \approx 0.03$) to high ($z \approx 3.1$) redshift. Figure 1 also shows the highest-energy photons detected from the blazars in our sample.

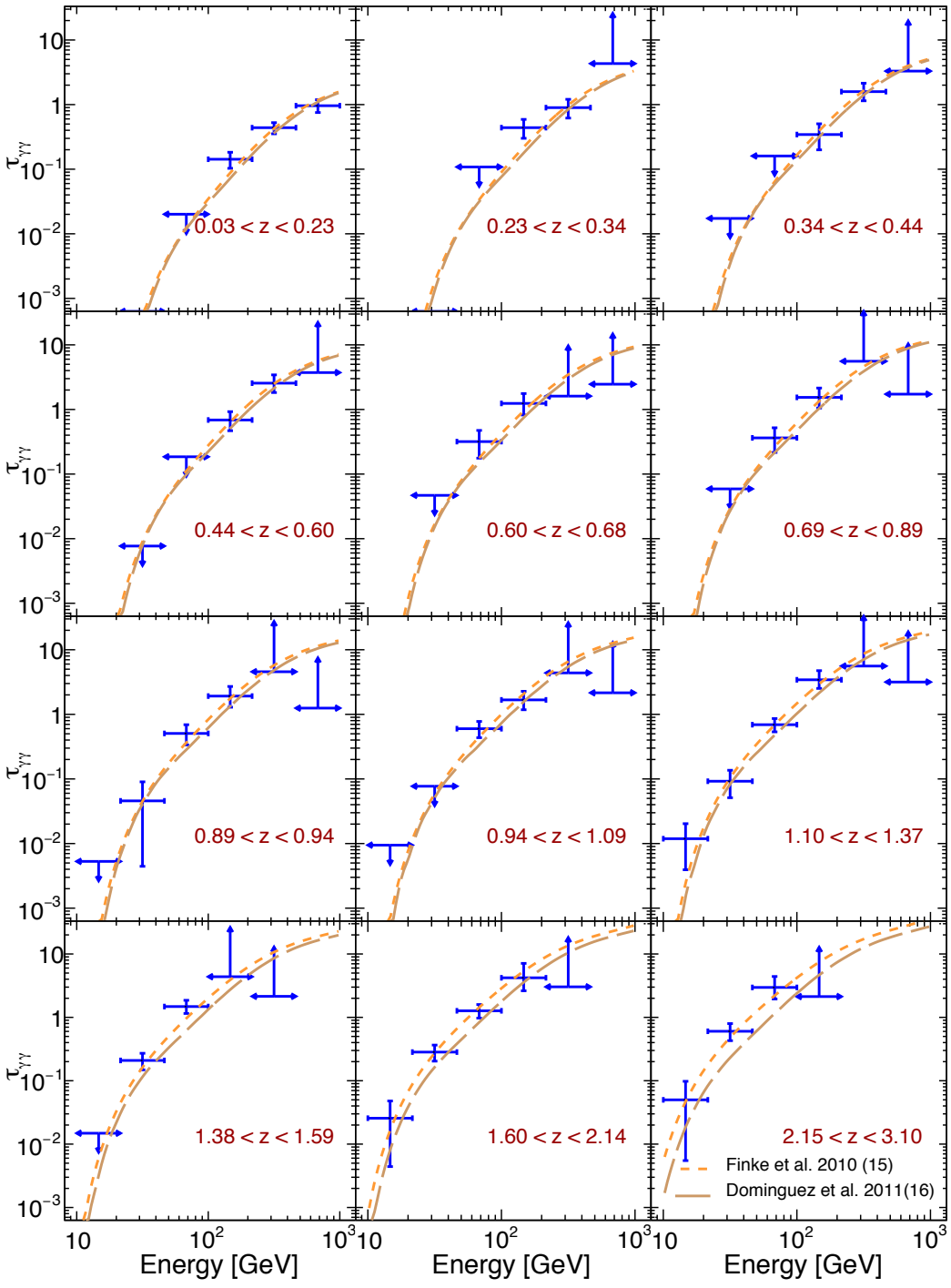

Figure S3 **Measurements of the optical depth $\tau_{\gamma\gamma}$ due to the EBL in different redshift and energy bins.** The lines show the predictions of two EBL models (*29, 37*).

GRB 080916C

In order to constrain the EBL and SFH to the highest possible redshifts, we complement the blazar sample with a single gamma-ray burst (GRB), GRB 080916C, detected by *Fermi* LAT at z=4.35 (*30, 58*). This was an extremely luminous event, whose hard spectrum has already produced constraints on the SFH at high redshift (*59, 60*). With respect to previous works, the release of the Pass 8 event-level analysis has allowed us to recover more high-energy photons, particularly one at 27.4 GeV, ≈146 GeV in the source frame, from GRB 080916C (*61*).

The analysis is similar to the one reported by (*62*). Transient-class photons between 0.1 GeV and 100 GeV were downloaded around a 10° position from the burst and from the time of the GRB until 1775.9 s later. Photons detected at a zenith angle greater than 105° were removed. The ROI model consists of the burst, the Galactic and isotropic templates (*63*). We rely on the 'P8R2_TRANSIENT020' IRF.

The source intrinsic spectrum is represented (and fitted up to 10 GeV) by a single power law (with a photon index of 2.25 ± 0.06) employing a time-averaged analysis. No curvature is observed in the *Fermi*-LAT spectrum. A time-resolved analysis does not yield any difference for this work (*62*). We produce a 95 % upper limit on the optical depth by adopting the same method as described above for blazars. This upper limit is $\tau_{\gamma\gamma} < 0.46$ at an energy of ≈17 GeV and z=4.35 and it does not depend on the EBL model used to derive it. This upper limit is a factor of two lower than that used by (*60*). This is due to the additional photons detected at >10 GeV and particularly to the 27.4 GeV photon. The probability that this photon belongs to the background, rather than to GRB 080916C, is only 5×10^{-5}. A so-called 'maximally conservative upper limit' based on the assumption that the intrinsic spectrum cannot be harder than a power law with an index $\Gamma = 1.5$ is even more constraining; however, it is not adopted here. The spectrum of GRB 080916C used here is shown in Figure S4.

Tests and Simulations

Simulations of Blazar SEDs

The analysis chain described in the previous section has first been tested and optimized on Monte Carlo simulation of synthetic spectral-energy distributions (SEDs) of blazars with properties matching those of blazars observed by *Fermi* LAT.

The SEDs are generated from physical models of blazars' emission that include synchrotron and synchrotron self-Compton as well as (for FSRQs) external Compton scattering and were generated with the numerical code presented in (*64*) and (*65*). These SEDs reproduce the range of peak frequencies very well (for both the synchrotron and γ-ray components), including peak curvatures and γ-ray photon indices observed in both *Fermi*-LAT BL Lacs and FSRQs. They include all known effects that contribute to determining the curvature of the intrinsic γ-ray spectrum of *Fermi* blazars. The crucial transition from the Thomson to the Klein-Nishina cross section as well as (mostly important for FSRQs) absorption within the broad line region (for

Table S3. EBL Optical Depths $\tau_{\gamma\gamma}$ in bins of redshift and energy as reported in Figure S3.

$\bar{z}$	z_{min}	z_{max}	[10.0-21.4] (GeV)	[21.4-46.4] (GeV)	[46.4-100.0] (GeV)	[100.0-215.4] (GeV)	[215.4-464.1] (GeV)	[464.1-1000] (GeV)
0.14	0.03	0.23	$\cdots$	$\cdots$	< 0.02	$0.14^{+0.04}_{-0.04}$	$0.44^{+0.09}_{-0.09}$	$0.96^{+0.23}_{-0.21}$
0.27	0.23	0.34	$\cdots$	$\cdots$	< 0.11	$0.44^{+0.15}_{-0.14}$	$0.90^{+0.31}_{-0.28}$	> 4.32
0.39	0.34	0.44	$\cdots$	< 0.02	< 0.16	$0.34^{+0.16}_{-0.14}$	$1.59^{+0.56}_{-0.44}$	> 3.30
0.52	0.44	0.60	$\cdots$	< 0.01	< 0.19	$0.69^{+0.24}_{-0.22}$	$2.55^{+0.88}_{-0.73}$	> 3.72
0.65	0.60	0.68	$\cdots$	< 0.05	$0.32^{+0.16}_{-0.14}$	$1.24^{+0.52}_{-0.42}$	> 1.61	> 2.46
0.79	0.69	0.89	$\cdots$	< 0.06	$0.36^{+0.16}_{-0.15}$	$1.54^{+0.61}_{-0.49}$	> 5.57	> 1.73
0.92	0.89	0.94	< 0.01	$0.05^{+0.04}_{-0.04}$	$0.51^{+0.18}_{-0.17}$	$1.92^{+0.78}_{-0.63}$	> 4.56	> 1.25
1.01	0.94	1.09	< 0.01	< 0.08	$0.60^{+0.18}_{-0.16}$	$1.67^{+0.60}_{-0.50}$	> 4.38	> 2.16
1.24	1.10	1.37	$0.01^{+0.01}_{-0.01}$	$0.09^{+0.04}_{-0.04}$	$0.69^{+0.17}_{-0.16}$	$3.43^{+1.32}_{-0.91}$	> 5.59	> 3.16
1.47	1.38	1.59	< 0.01	$0.21^{+0.06}_{-0.06}$	$1.48^{+0.38}_{-0.33}$	> 4.38	> 2.15	$\cdots$
1.82	1.60	2.14	$0.03^{+0.02}_{-0.02}$	$0.28^{+0.08}_{-0.08}$	$1.27^{+0.32}_{-0.30}$	$4.21^{+2.90}_{-1.59}$	> 3.03	$\cdots$
2.40	2.15	3.10	$0.05^{+0.05}_{-0.04}$	$0.60^{+0.19}_{-0.17}$	$2.97^{+1.45}_{-1.02}$	> 2.13	$\cdots$	$\cdots$

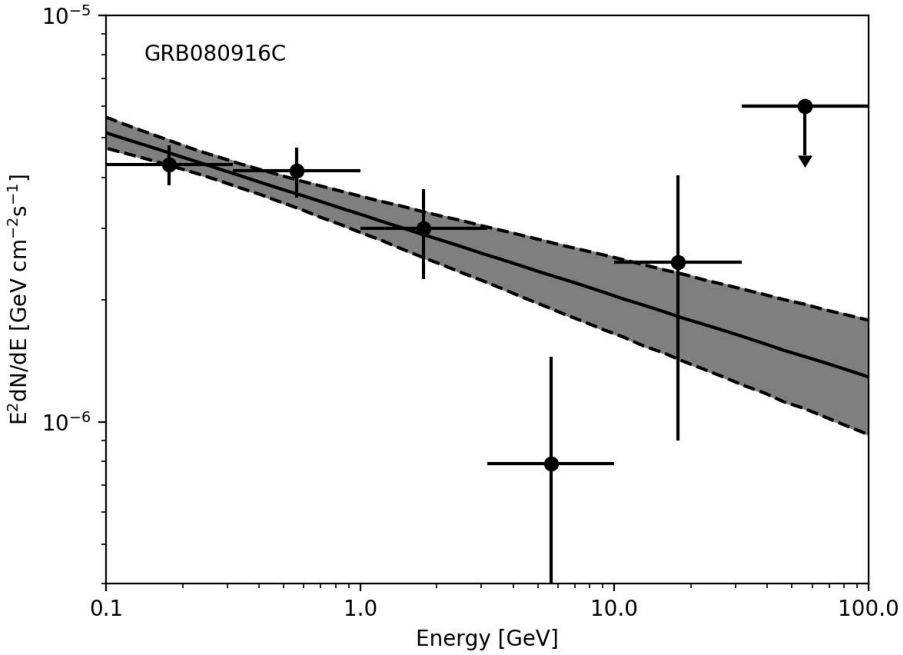

Figure S4 **Spectrum of GRB 080916C between 0.1 GeV and 100 GeV.** The solid line and shaded region represent the best-fitting power-law model and its 1 σ uncertainty, respectively.

different distances of the emission region from the broad line region) are all taken into account and contribute to determine the shape of the blazars' spectra at high energy.

These SEDs, attenuated by the EBL for a range of redshifts similar to those of Figure S1, are then used to simulate LAT observations of these synthetic sources and have been used to optimize the analysis set-up presented above. In particular, the values of the minimum energy ($E_{\rm min}$=1 GeV) and those of $TS_{\rm c,1}$ and $TS_{\rm c,2}$ have been derived from the analysis of simulations. Figure S5 shows that the analysis chain employed in this work can effectively recover the simulated level of EBL.

Variability

Blazars are inherently variable objects (at all wavelengths) and variability may bias or complicate the measurement of the EBL attenuation. In order to cope with blazars' variability as much as possible, a time-resolved analysis is performed for all sources that are found variable at > 10 GeV in the recent third catalog of hard sources, 3FHL, (*66*). We rely on the time bins derived by the Bayesian block analysis presented in 3FHL as these are times when the sources were found to alter their state at > 10 GeV, which is the relevant energy range for detecting the

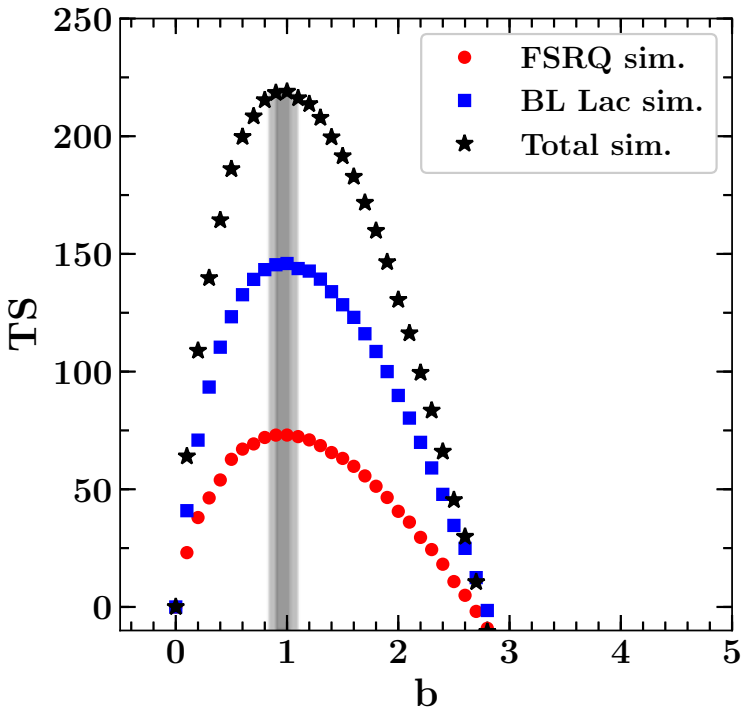

Figure S5 **Detection of the EBL attenuation in Monte Carlo simulations.** Test statistics of the EBL as a function of the scaling parameter b adopting the model of (*29*) for our set of Monte Carlo simulations. The shaded regions show the 1 σ and 2 σ confidence intervals around the best fit.

EBL attenuation. In each time bin, the criteria reported in Table S1 are used to determine the best intrinsic spectral model. Because for a given source time-resolved spectra can be treated as independent observations, their contribution to the $TS_{\rm EBL}$ has been summed to the one of the remainder of the sample. Figure S2 includes the contribution from variable and non-variable sources. The level of EBL as determined from the variable sources alone is found to be in good agreement with the rest of the sample. Figure S6 shows the $TS_{\rm EBL}$ as a function of the b parameter (for the model of (*29*)) for 4 variable BL Lacs and FSRQs and how that compares to the result of a time-averaged analysis. In general, we find a time-averaged analysis works well for objects which vary primarily in flux, while a time-resolved analysis is required for all those objects experiencing also spectral variability (see right versus left plots in Figure S6). Finally, we used the Fermi All-sky Variability Analysis tool (*67, 68*) to search for significant residual spectral variability within Bayesian blocks, but none could be found.

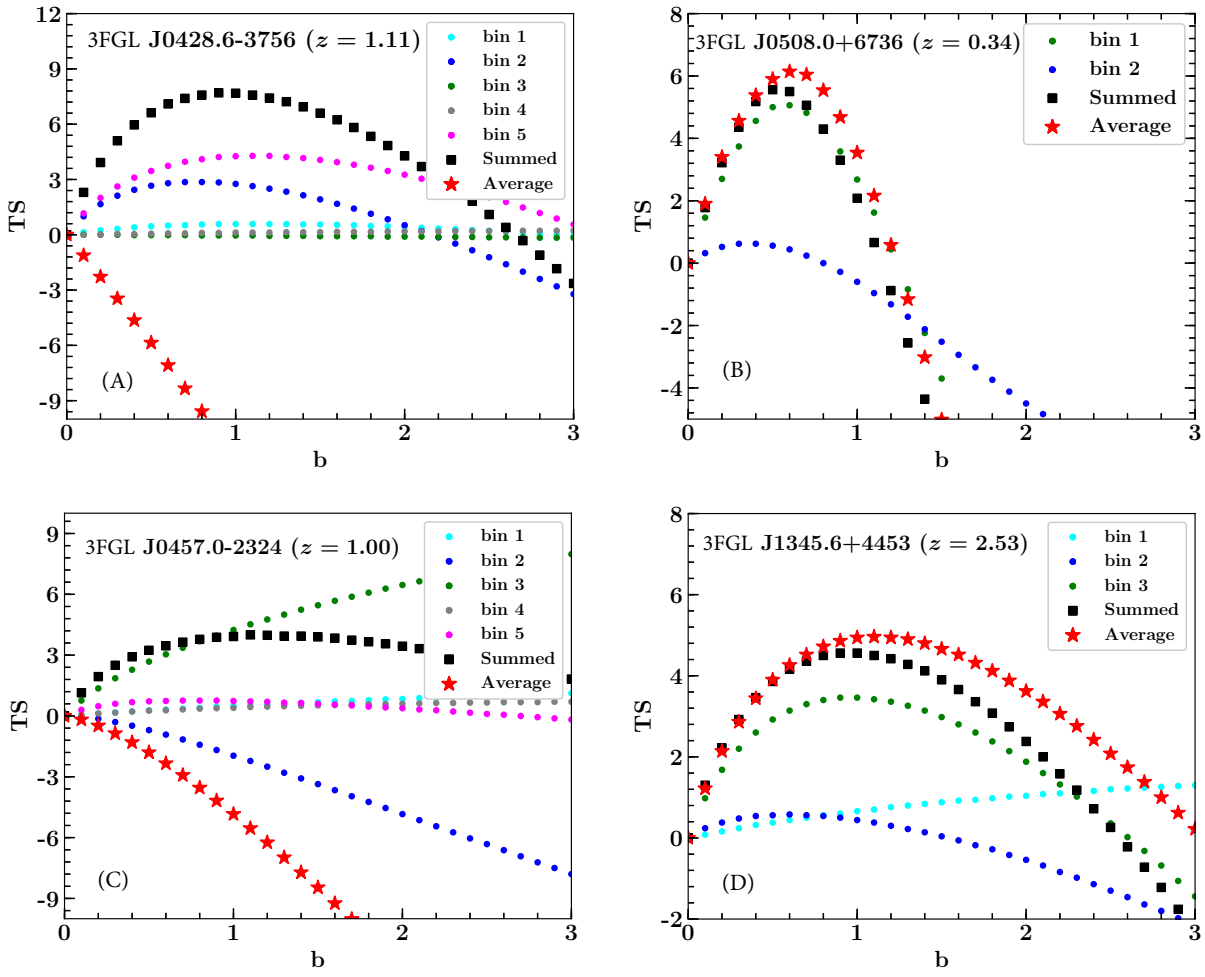

Figure S6 **Impact of time-resolved analysis.** Contribution to the $TS_{\rm EBL}$ as a function of scaling parameter b, adopting the model of (*29*), for the time resolved (Summed) and time averaged (Average) analysis for two BL Lacs (top) and two FSRQs (bottom).

Systematic Uncertainties

In order to gauge the systematic uncertainties of this analysis we have performed the tests reported below:

- Instead of using a variable maximum energy up to which to fit the intrinsic spectrum (chosen to be the energy corresponding to $\tau_{\gamma\gamma} < 0.1$ for the model of (*29*)), we use a constant maximum energy of 10 GeV for all sources. Repeating the entire analysis we find $b = 1.09 \pm 0.08$ in agreement with the results presented in the main text.

- A similar result as above has been obtained using a maximum energy, to measure the

intrinsic spectrum, defined as that obtained when $\tau_{\gamma\gamma} < 0.05$ ($b = 1.07 \pm 0.08$ for the model of (*29*)).

- We use the IRF bracketing method as described in (*69*). By deriving two different sets of IRFs and repeating the entire analysis we find that the systematic uncertainty in the optical depth $\tau_{\gamma\gamma}$ is of the order $\sim$7 %.

The results presented in the above sections are fully confirmed and the systematic uncertainty on the optical depth $\tau_{\gamma\gamma}$ due to changing the energy threshold to characterize the intrinsic spectrum and IRF are, together, $\lesssim$10 %. A systematic uncertainty of $0.1 \times \tau_{\gamma\gamma}$ (added in quadrature) has been included in the uncertainties reported in Figures 1 and S3 and propagated to all results that use those data.

Reconstructing the evolving EBL

The optical depth for a γ ray of observed energy E_γ originating in a source at redshift z_s is related to the evolving number density of EBL photons, $n_{\rm EBL}(\epsilon, z)$, (*70–72*):

$$\tau_{\gamma\gamma}(E_\gamma, z_s) = c \int_0^{z_s} \left|\frac{dt}{dz}\right| dz \int_{-1}^{1} (1-\mu)\frac{d\mu}{2} \int_{2m_e^2c^4/\epsilon_\gamma(1-\mu)}^{\infty} \sigma(\epsilon_{\rm EBL}, \epsilon_\gamma, \mu) n_{\rm EBL}(\epsilon, z) d\epsilon_{\rm EBL} \quad \text{(S5)}$$

where the rest-frame energy of γ rays and EBL photons are denoted by $\epsilon_\gamma = E_\gamma(1+z_s)$ and $\epsilon_{\rm EBL} = E_{\rm EBL}(1+z_s)$ respectively, $\mu = \cos\theta$ denotes the angle of incidence between the two photons, and $|dt/dz|^{-1} = H_0(1+z)\sqrt{\Omega_M(1+z)^3+\Omega_\Lambda}$, where the Hubble and the cosmological parameters are $H_0 = 70\,{\rm km\ s^{-1}\ Mpc^{-1}}$, Ω_M=0.3, and Ω_λ =0.7. The cross section for the photon-photon interaction appearing in the last integral in Equation S5 is

$$\sigma(\epsilon_{\rm EBL}, \epsilon_\gamma, \mu) = \frac{3\sigma_T}{16}(1-\beta^2)\left[2\beta(\beta^2-2) + (3-\beta^4)\ln\left(\frac{1+\beta}{1-\beta}\right)\right], \quad \text{(S6)}$$

with

$$\beta = \sqrt{1 - \frac{2m_e^2c^4}{\epsilon_{\rm EBL}\epsilon_\gamma(1-\mu)}}.$$

where $m_e c^2$ is the electron rest mass. In other words, for a given cosmology, the SED and evolution of the EBL uniquely specify the optical depth at all redshifts. Conversely, we can use the measured optical depths $\tau_{\gamma\gamma}(E_\gamma, z)$ to reconstruct $n_{\rm EBL}(\epsilon, z)$.

The physical properties of galaxies, such as star-formation rate, stellar mass and metallicity, are encoded in their SED. Rather than the EBL, which is accumulated over cosmic time, it is more informative to study the instantaneous SED of the galaxy population as a whole i.e.,

the cosmic emissivity. The buildup of the EBL is related to the volume emissivity $j(\epsilon, z)$ (or equivalently, luminosity density) via:

$$n_{\rm EBL}(\epsilon, z) = (1+z)^3 \int_z^\infty \frac{j(\epsilon', \bar{z})}{\epsilon'} \left| \frac{dt}{d\bar{z}} \right| d\bar{z}, \tag{S7}$$

where $\epsilon' = \epsilon(1+\bar{z})$ is the rest-frame energy at $\bar{z}$. The EBL spectral intensity (see Figure 2) can be found from the number density by $\epsilon I(\epsilon, z) = \frac{c}{4\pi}\epsilon^2 n_{\rm EBL}(\epsilon, z)$.

Model for the Cosmic Emissivity

Our task is to reconstruct $j(\epsilon, z)$ based on the measured optical depths reported in Figure S3 without making assumptions on galaxy properties or their stellar population. We represent $j(\lambda)$ as the sum of several log-normal templates with a fixed peak position:

$$j(\lambda) = \sum_i a_i \cdot \exp\left[-\frac{(\log\lambda - \log\lambda_i)^2}{2\sigma^2} \right] \quad [\mathrm{erg \cdot s^{-1} cm^{-3} Hz^{-1}}] \tag{S8}$$

where we fix $\sigma = 0.2$, $\lambda_i = [0.17, 0.92, 2.2, 8.0]\,\mu\mathrm{m}$ and the amplitudes a_i are left free to vary. We find that four log-normal templates allow for a sufficiently flexible spectral shape from UV to the mid-IR. A Lyman-break is imposed by cutting off the spectrum at $\epsilon > 13.6\,\mathrm{eV}$ where neutral hydrogen becomes opaque. We have chosen the fixed locations (λ_i) and width (σ) of the templates such that common features in galaxy SEDs, a flat far-UV continuum and a 4000Å/Balmer break, are easily captured. Each template is allowed to evolve independently with redshift based on a function similar to the SFH parametrization of (*1*) leading to the full expression

$$j(\lambda_i, z) = \sum_i a_i \cdot \exp\left[-\frac{(\log\lambda - \log\lambda_i)^2}{2\sigma^2} \right] \times \frac{(1+z)^{b_i}}{1 + \left(\frac{1+z}{c_i}\right)^{d_i}}. \tag{S9}$$

At each of the fixed wavelengths λ_i, one parameter controls the amplitude, a_i, and three control the evolution, b_i, c_i and d_i, yielding a total of $4 \times 4 = 16$ free parameters. The number of optical depth data points is 60.

To explore the sensitivity to different functional forms for the evolution, we also test the parametrization from (*73*):

$$j(\lambda_i, z) \propto \frac{a_i + b_i z}{1 + (z/c_i)^{d_i}}\ , \tag{S10}$$

with free parameters a_i, b_i, c_i, and d_i which we display alongside our main results for the SFH in Figure S11.

Markov Chain Monte Carlo: Setup

We use the MCMC code `emcee` (*74*), a Python implementation of an affine invariant MCMC ensemble sampler (*75*), to constrain the parameters controlling the emissivity. The likelihood function is estimated as $\mathscr{L} \propto \exp(-\chi^2)$ where χ^2 is given by

$$\chi^2 = \sum_{i=1}^{N}\sum_{j=1}^{M} \frac{[\tau_{\rm data}(E_i, z_j) - \tau_{\rm model}(\vec{\theta}|E_i, z_j)]^2}{\sigma_{i,j}^2} \tag{S11}$$

where there are N energy (E_i) bins, M redshift (z_j) bins, $\tau_{\rm data}(E_i, z_j)$ is the measured absorption optical depth presented in Figure S3, $\tau_{\rm model}(\vec{\theta}|E_i, z_j)$ is the model absorption optical depth with parameters $\vec{\theta}$, and $\sigma_{i,j}$ is the (statistical plus systematic) uncertainty on the absorption optical depth measurements.

We choose flat priors on all parameters $\log a_i/(\mathrm{ergs^{-1}Mpc^{-3}Hz^{-1}}) = [22, 32]$, $b_i = [-2, 10]$, $c_i = [1, 7]$, $d_i = [0, 20]$. We restrict the range of the evolution parameter controlling the location of the peak (or curvature) to $c_i = [1, 7]$ since our dataset has limited constraining power for shape changes at redshifts much larger than our sample coverage ($0 < z < 4$). Note however, that this does not force the presence of a peak and a turnover as the function reduces to a power-law $\propto (1+z)^{b_i}$ when $d \to 0$.

With the emissivity specified as a function of wavelength and redshift, we calculate the resulting EBL and optical depth according to Equations S5–S7 respectively for each proposed step in the MCMC. Each calculation of $\tau_{\gamma\gamma}$ involves integrating over wavelength, redshift and angle of incidence, but we only require $\tau_{\gamma\gamma}$ at six energies, for every redshift, making it computationally manageable. Our final results are based on MCMC chains from 120 walkers exploring the parameter space in 10,000 steps each. This results in 1,140,000 steps after a burn-in of 500 steps for each walker.

Results and Validation

In Figure S7 we display the 68% and 95% confidence regions for the total cosmic emissivity in several redshift bins. The *Fermi*-LAT dataset is tightly constraining at UV, optical and, at low-z, also near-IR wavelengths. The confidence regions get broader towards mid-IR wavelengths due to the energy range of *Fermi* LAT being limited to < 1 TeV. Figure S7 also shows that the *Fermi*-LAT dataset provides the tightest constraints around $z \simeq 0.5 - 1.5$ as the opacity increases for larger distances traveled. At $z \gtrsim 2$ we are limited by the number of bright blazars with substantial emission above $\sim$10 GeV in our sample. Comparing our cosmic emissivity with measurements of integrated galaxy luminosity functions shows that our results are in good overall agreement across the wavelength range. This implies that the bulk of the EBL is already accounted for by galaxy surveys.

We have validated this reconstruction method by creating ten sets of fake $\tau(E, z)$ data points in the same energy and redshift bins, and possessing the same fractional uncertainties, as the

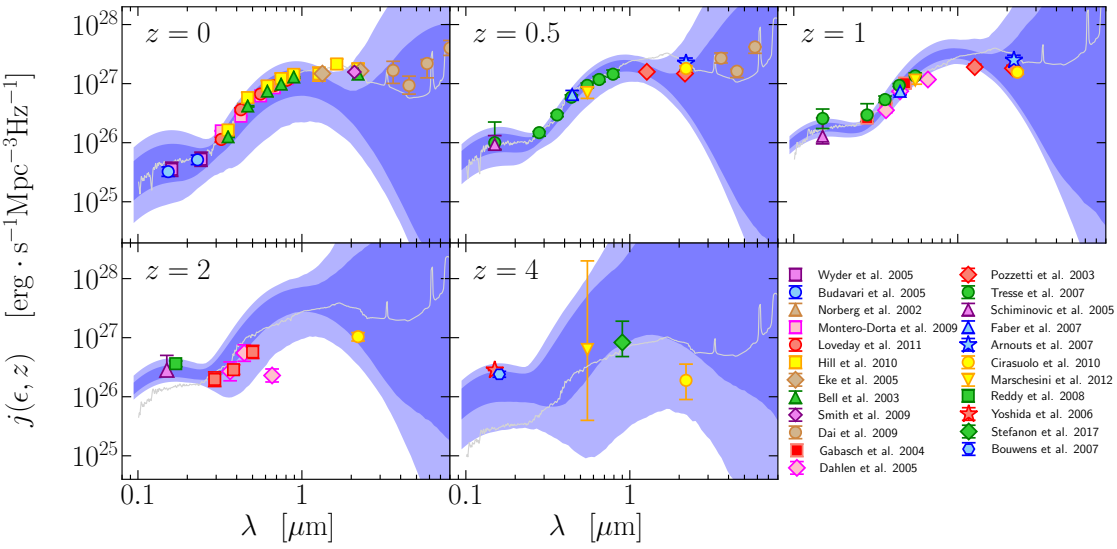

Figure S7 **The cosmic emissivity (luminosity density) as a function of wavelength in several redshift slices.** The blue shaded regions correspond to the $1\,\sigma$ and $2\,\sigma$ confidence regions resulting from the empirical EBL reconstruction method. The data points are independent measurements from integrated galaxy luminosity functions in the literature. We have not corrected the data for evolution from the redshift displayed (e.g. $z = 1$ panel shows measurements at $0.9 < z < 1.15$) which may cause some additional scatter. Our results are in general agreement with the galaxy survey data. The gray lines correspond to the EBL model of (*37*) where the luminosity density is found to be dominated by a spiral-type galaxy SED template.

original dataset. The simulated datasets are generated by drawing random sets of values for the 16 parameters of Equation S9, within their assumed priors, and calculating the optical depths at each energy and redshift bin. Our reconstruction recovers the fake EBL in all cases within the derived $2\,\sigma$ uncertainty region. We see no evidence for a systematic over- or underestimation of the emissivity at any particular wavelength. The largest offsets arise at $> 1\mu\mathrm{m}$ where the dataset is less constraining.

Comparison with EBL models and data

The literature offers different approaches to estimate the evolving EBL . There are methodologies that are observationally motivated (*15, 37, 38, 52, 76*), physically motivated (*29, 55, 77, 78*), and based on semi-analytical models of galaxy formation such as (*51, 54*). Typically these models are constructed in such a way that the lower redshifts and, in general, the optical/near-IR peak are better constrained. Figure S8 shows our reconstructed EBL spectral intensities in comparison with some of the models.

The reconstructed EBL follows galaxy counts (*18, 19*) leaving little room for substantial contributions not resolved by deep galaxy surveys. This is in conflict with several direct measurements of EBL (which may be contaminated by foregrounds, see e.g. (*22, 79, 80*)) and in tension with some models proposed to explain the anisotropies measured in diffuse light (*23*).

Relative to EBL models, in the local Universe, we find that our estimate roughly follows the median of existing models. The models by (*29*), (*55*), (*37*), (*38*), and (*52*) reproduce our results quite well. The fiducial model by (*51*) tends to follow the upper region of our 1σ band. Finally, the baseline model by (*54*) provides too much UV and too little near-IR.

The strategy of using the observation of γ-ray photons to derive constraints on the background has been used extensively in recent years. Early attempts, characterized by scarcer γ-ray data, only allowed intensity upper limits as a consequence of assumptions on the intrinsic spectra of blazars (*42, 81, 82*). These results were followed by more sophisticated approaches based on more and better data that allowed the EBL detection and study, both with the LAT at somewhat lower energies and thus, larger redshifts (*13, 62, 83, 84*), and with Imaging Atmospheric Cherenkov Telescopes (IACTs). These results from IACTs mostly constrain the local Universe (*39–41*), although the MAGIC collaboration also probed the EBL at $z \sim 1$ with the detection of two blazars (*85, 86*). Notably, our derived EBL at $z = 0$ is even closer to the integrated counts compared to previous γ-ray derived EBL measurements.

Table S4 reports the EBL spectral intensities at several redshifts as displayed in Figure 2. Using Equation S5, we can calculate the optical depth curves as a function of energy and redshift from our reconstructed EBL. These can be used to correct spectra of cosmological γ-ray sources for EBL absorption in order to study physical properties of the source and are provided online.

Table S4. Spectral intensity[a] (λI_λ) of the EBL as a function of redshift and wavelengths as reported in Figure 2. The intensities reported in the this table are in comoving coordinates. To reproduce the results of Figure 2 (shown in physical coordinates) they need to be multiplied by a $(1+z)^3$ factor. A machine-readable version of this table is provided in Data S1 and online.

λ (μm)	$z=0$ (nW m^{-2} sr^{-1})	$z=1$ (nW m^{-2} sr^{-1})	$z=2$ (nW m^{-2} sr^{-1})	$z=3$ (nW m^{-2} sr^{-1})
0.102	$0.12^{+0.12}_{-0.07}$	$0.41^{+0.08}_{-0.06}$	$0.36^{+0.11}_{-0.07}$	$0.21^{+0.07}_{-0.08}$
0.111	$0.33^{+0.31}_{-0.20}$	$0.90^{+0.18}_{-0.13}$	$0.72^{+0.20}_{-0.14}$	$0.39^{+0.14}_{-0.15}$
0.120	$0.59^{+0.51}_{-0.34}$	$1.42^{+0.29}_{-0.21}$	$1.05^{+0.28}_{-0.21}$	$0.55^{+0.21}_{-0.23}$
0.130	$0.90^{+0.68}_{-0.49}$	$1.92^{+0.38}_{-0.29}$	$1.33^{+0.36}_{-0.28}$	$0.68^{+0.28}_{-0.30}$
0.141	$1.22^{+0.83}_{-0.63}$	$2.37^{+0.44}_{-0.37}$	$1.55^{+0.40}_{-0.34}$	$0.78^{+0.34}_{-0.35}$
0.153	$1.55^{+0.92}_{-0.74}$	$2.74^{+0.50}_{-0.43}$	$1.71^{+0.45}_{-0.38}$	$0.84^{+0.39}_{-0.39}$
0.166	$1.87^{+0.98}_{-0.84}$	$2.99^{+0.56}_{-0.46}$	$1.80^{+0.47}_{-0.42}$	$0.87^{+0.43}_{-0.42}$
0.180	$2.16^{+0.99}_{-0.87}$	$3.15^{+0.59}_{-0.48}$	$1.82^{+0.48}_{-0.44}$	$0.87^{+0.45}_{-0.42}$
0.195	$2.44^{+0.93}_{-0.89}$	$3.21^{+0.58}_{-0.48}$	$1.79^{+0.47}_{-0.45}$	$0.84^{+0.46}_{-0.42}$
0.212	$2.68^{+0.87}_{-0.86}$	$3.19^{+0.55}_{-0.47}$	$1.72^{+0.46}_{-0.44}$	$0.80^{+0.45}_{-0.41}$
0.230	$2.86^{+0.79}_{-0.79}$	$3.10^{+0.50}_{-0.44}$	$1.62^{+0.45}_{-0.42}$	$0.75^{+0.45}_{-0.38}$
0.249	$3.01^{+0.70}_{-0.69}$	$2.98^{+0.45}_{-0.40}$	$1.52^{+0.43}_{-0.40}$	$0.71^{+0.42}_{-0.36}$
0.270	$3.12^{+0.60}_{-0.56}$	$2.85^{+0.41}_{-0.36}$	$1.44^{+0.40}_{-0.39}$	$0.68^{+0.39}_{-0.35}$
0.293	$3.23^{+0.50}_{-0.48}$	$2.75^{+0.38}_{-0.33}$	$1.40^{+0.38}_{-0.39}$	$0.66^{+0.41}_{-0.36}$
0.318	$3.33^{+0.44}_{-0.41}$	$2.72^{+0.34}_{-0.32}$	$1.39^{+0.42}_{-0.43}$	$0.68^{+0.46}_{-0.39}$
0.345	$3.46^{+0.41}_{-0.42}$	$2.77^{+0.38}_{-0.35}$	$1.45^{+0.52}_{-0.53}$	$0.70^{+0.56}_{-0.43}$
0.374	$3.63^{+0.46}_{-0.48}$	$2.96^{+0.44}_{-0.43}$	$1.57^{+0.71}_{-0.65}$	$0.74^{+0.75}_{-0.48}$
0.405	$3.87^{+0.59}_{-0.62}$	$3.27^{+0.57}_{-0.56}$	$1.77^{+0.96}_{-0.83}$	$0.84^{+0.98}_{-0.58}$
0.440	$4.21^{+0.75}_{-0.80}$	$3.73^{+0.72}_{-0.77}$	$2.04^{+1.28}_{-1.06}$	$0.99^{+1.26}_{-0.72}$
0.477	$4.64^{+0.92}_{-0.98}$	$4.34^{+0.94}_{-1.01}$	$2.38^{+1.69}_{-1.33}$	$1.20^{+1.63}_{-0.92}$
0.517	$5.19^{+1.12}_{-1.20}$	$5.06^{+1.20}_{-1.27}$	$2.80^{+2.12}_{-1.63}$	$1.47^{+2.09}_{-1.18}$
0.561	$5.84^{+1.32}_{-1.42}$	$5.91^{+1.48}_{-1.57}$	$3.27^{+2.58}_{-1.95}$	$1.78^{+2.66}_{-1.45}$
0.608	$6.59^{+1.50}_{-1.65}$	$6.81^{+1.77}_{-1.93}$	$3.79^{+3.07}_{-2.28}$	$2.13^{+3.32}_{-1.75}$
0.660	$7.41^{+1.67}_{-1.87}$	$7.71^{+2.14}_{-2.23}$	$4.32^{+3.55}_{-2.60}$	$2.47^{+4.35}_{-2.06}$
0.716	$8.25^{+1.82}_{-2.02}$	$8.56^{+2.50}_{-2.55}$	$4.88^{+4.01}_{-2.95}$	$2.88^{+5.38}_{-2.41}$
0.776	$9.09^{+1.90}_{-2.13}$	$9.30^{+2.87}_{-2.84}$	$5.48^{+4.56}_{-3.35}$	$3.27^{+6.58}_{-2.72}$
0.842	$9.88^{+1.95}_{-2.16}$	$9.90^{+3.23}_{-3.09}$	$5.98^{+5.15}_{-3.72}$	$3.64^{+7.78}_{-3.02}$
0.913	$10.60^{+1.96}_{-2.18}$	$10.32^{+3.56}_{-3.18}$	$6.52^{+5.88}_{-4.14}$	$3.94^{+9.86}_{-3.25}$
0.990	$11.15^{+1.88}_{-2.06}$	$10.60^{+3.84}_{-3.36}$	$6.83^{+6.60}_{-4.40}$	$4.26^{+12.24}_{-3.52}$
1.074	$11.54^{+1.79}_{-1.90}$	$10.73^{+4.04}_{-3.48}$	$6.97^{+7.81}_{-4.51}$	$4.51^{+15.08}_{-3.73}$
1.164	$11.79^{+1.65}_{-1.76}$	$10.64^{+4.23}_{-3.47}$	$7.04^{+9.00}_{-4.55}$	$4.65^{+19.68}_{-3.87}$
1.263	$11.86^{+1.50}_{-1.58}$	$10.46^{+4.47}_{-3.65}$	$6.91^{+11.27}_{-4.47}$	$4.72^{+28.24}_{-3.94}$
1.370	$11.73^{+1.40}_{-1.41}$	$10.05^{+4.94}_{-3.72}$	$6.87^{+13.94}_{-4.59}$	$4.79^{+40.34}_{-4.00}$

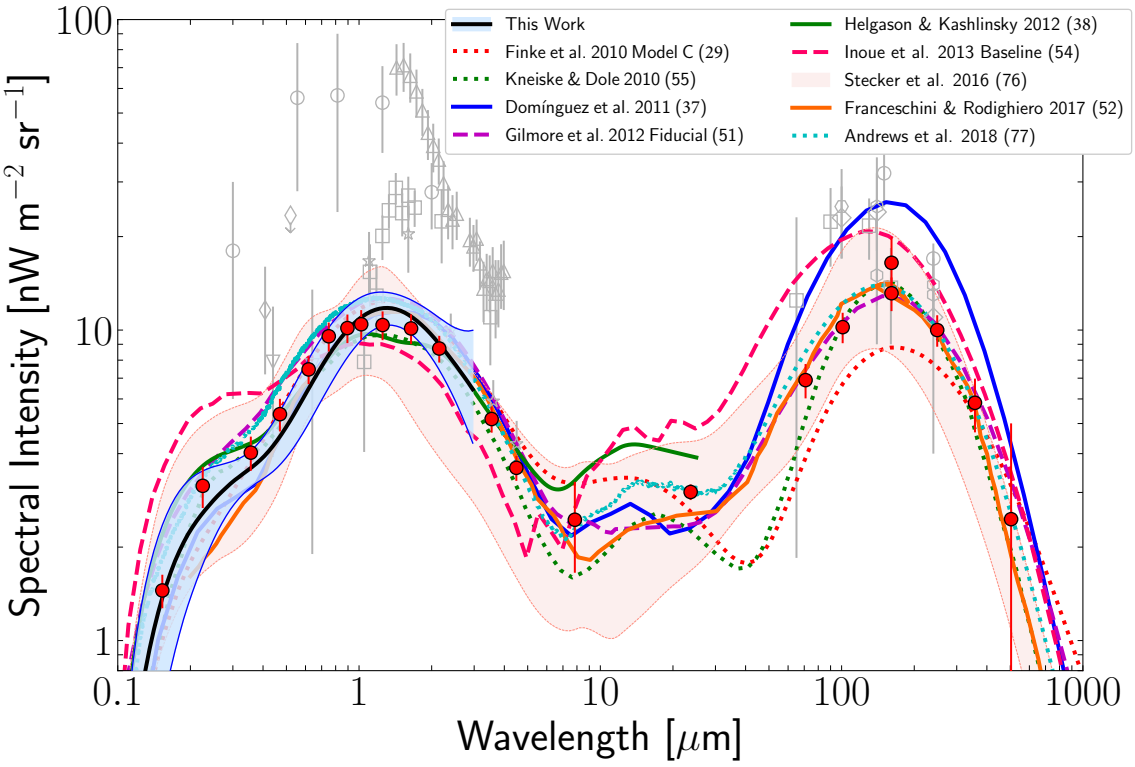

Figure S8 **SED of the EBL at** $z = 0$**.** Recovered EBL spectral energy distribution at $z = 0$ (solid black line) with its 1σ uncertainties (shaded blue) in comparison with the some estimates from empirical models from ultraviolet to far-IR wavelengths. We show some examples for different modeling methodologies: observationally motivated (solid lines), physically motivated (dotted lines), and theoretically motivated (dashed lines). Our uncertainties start to diverge above the near-IR as a consequence of the larger uncertainties of our optical-depth data at the larger γ-ray energies. A compilation of data from direct detection (open gray symbols) and galaxy counts (filled red symbols, (*15*)) is also shown. Our spectral intensities match those results from galaxy counts leaving little room for substantial contributions from sources that have not been detected in deep surveys.

Table S4 (cont'd)

λ (μm)	$z = 0$ (nW m^{-2} sr^{-1})	$z = 1$ (nW m^{-2} sr^{-1})	$z = 2$ (nW m^{-2} sr^{-1})	$z = 3$ (nW m^{-2} sr^{-1})
1.485	$11.50^{+1.28}_{-1.38}$	$9.56^{+5.80}_{-3.78}$	$6.81^{+18.49}_{-4.68}$	$4.81^{+58.87}_{-4.05}$
1.611	$11.07^{+1.35}_{-1.35}$	$9.09^{+6.77}_{-3.86}$	$6.52^{+25.41}_{-4.61}$	$4.67^{+84.71}_{-3.96}$
1.747	$10.53^{+1.46}_{-1.42}$	$8.54^{+8.48}_{-3.96}$	$6.20^{+37.72}_{-4.52}$	$4.51^{+117.34}_{-3.86}$
1.895	$9.94^{+1.63}_{-1.53}$	$7.97^{+10.94}_{-4.01}$	$5.77^{+55.07}_{-4.28}$	$4.38^{+156.29}_{-3.84}$
2.055	$9.34^{+1.87}_{-1.70}$	$7.57^{+14.47}_{-4.07}$	$5.51^{+76.16}_{-4.22}$	$4.40^{+213.73}_{-3.90}$
2.229	$8.72^{+2.14}_{-1.86}$	$7.01^{+20.41}_{-4.10}$	$5.38^{+101.00}_{-4.31}$	$4.47^{+271.37}_{-4.03}$
2.417	$8.16^{+2.55}_{-2.03}$	$6.70^{+28.53}_{-4.28}$	$5.24^{+135.49}_{-4.33}$	$4.51^{+341.38}_{-4.11}$
2.621	$7.57^{+3.20}_{-2.16}$	$6.31^{+39.23}_{-4.30}$	$5.28^{+174.14}_{-4.50}$	$4.72^{+415.24}_{-4.37}$
2.843	$7.05^{+4.08}_{-2.33}$	$5.95^{+52.73}_{-4.31}$	$5.38^{+223.92}_{-4.71}$	$4.86^{+494.98}_{-4.55}$
3.083	$6.54^{+5.51}_{-2.48}$	...	...	...
3.344	$6.15^{+7.44}_{-2.69}$	...	...	...
3.626	$5.85^{+9.76}_{-2.91}$	...	...	...
3.933	$5.46^{+13.33}_{-3.03}$	...	...	...
4.265	$5.23^{+17.70}_{-3.21}$	...	...	...
4.626	$5.11^{+23.25}_{-3.44}$	...	...	...
5.017	$5.07^{+30.88}_{-3.70}$	...	...	...

Implications for the high-z Universe

In principle, there is always some constraining power beyond the maximum redshift of the sample of γ-ray sources. This is because the γ rays coming from $z_{\rm max}$ start interacting with EBL photons which were built up at still earlier times and the rate of the interactions is related to $n_{\rm EBL} \propto (1+z)^3$. Focusing on the UV, which is important for cosmic re-ionization, Figure S9 suggests rather minimal UV emissivity at $z > 4$ with respect to measurements from Lyman-break galaxy surveys. However, it is possible that the confidence regions at these redshifts may be artificially narrow due to the lack of flexibility in the parameterized shape of the evolution. In order to test the robustness of the constraints at high-z we have re-run the MCMC and included an additional term in Equation S9:

$$j_{\rm high-z}(\lambda, z) = a_{\rm high-z} \exp\left[-\frac{(z-z_0)^2}{2\sigma^2}\right] \left(\frac{\lambda}{0.17\mu{\rm m}}\right)^{-0.5} \tag{S12}$$

centered at $z_0 = 6$ with $\sigma = 0.08$. We find that, while this reveals a relatively unconstrained lower limit for the UV emissivity, the upper limit remains robust at $\sim 3.2(5.3) \times 10^{26}$ erg s^{-1} Mpc^{-3} Hz^{-1}, $1\sigma(2\sigma)$, at $z = 5-6$. In Figure 4, we compare this value with the integrated UV luminosity functions from the Hubble Frontier Fields (HFF) program, which targets extremely faint galaxies behind strong gravitational lenses, reaching $M_{\rm AB} \sim -13$. Some HFF analyses have found evidence for a turnover in the steep faint-end of the luminosity function (LF) (*35,36*), whereas others do not see such a feature (*33, 34*). The conflicting results at $M_{\rm AB} \gtrsim -15$ could be due to uncertainties in the magnification factor determined by lens models.

Our constraints limit how far a steep faint-end slope can be extrapolated. In fact, Figure 4 shows that the emissivities from the integrated UV luminosity functions are already close to our derived upper limits, but are all compatible within $2\,\sigma$. They favor a turnover of the LF at $M_{\rm AB} \sim -14$ in agreement with (*35*) and (*36*). The UV emissivity implied by (*34*) for example (with no turnover), would reach the 2σ upper limit if extrapolated to $M_{\rm AB} \sim -10$.

In Figure 4, we also show the UV emissivity necessary to sustain a reionized Universe at $z = 6$. The required emissivity (at 0.15 μm) can be shown to be (*87*):

$$j_{\rm UV} = 2.5 \times 10^{26}\ \epsilon_{53}^{-1} \left(\frac{1+z}{6}\right)^3 \left(\frac{\Omega_b h_{70}^2}{0.0461}\right)^2 \left(\frac{C/f_{\rm esc}}{30}\right)^2 \quad {\rm erg\ s^{-1} Mpc^{-3} Hz^{-1}}. \tag{S13}$$

Here, Ω_b is the cosmic baryon density, h_{70} is Hubble parameter in units of $70\,{\rm km\ s^{-1} Mpc^{-1}}$, C is the clumping factor of ionized hydrogen and $f_{\rm esc}$ is the mean escape fraction of ionizing photons. The parameter ϵ_{53} is the number of Lyman continuum photons per unit of forming stellar mass in units of 10^{53} photons $\cdot {\rm s^{-1}} ({\rm M_\odot \cdot yr^{-1}})^{-1}$. For this we follow (*88*) exploring values of ϵ_{53} based on stellar population synthesis models assuming a Salpeter IMF and a constant star formation rate. The width of the grey regions in Figure 4 correspond to the range $0.9 < \epsilon_{53} < 1.4$ when the metallicity is varied from $0.02 Z_\odot$ to $1.0 Z_\odot$ (where $Z_\odot$ is the solar metallicity). We display the emissivity for a reasonable assumption of $C/f_{\rm esc} = 30$, showing that our constraints accommodate a scenario in which the Universe is reionized at $z = 6$.

Our constraints at $z > 4$ come almost entirely from GRB 080916C which provides a strong upper limit to the optical depth at $z = 4.35$ whereas the blazar sample alone ($z < 3.1$) has lower constraining power. This is a benefit of detecting more high-z γ-ray sources as probes of the epoch of re-ionization (*89*).

The Star-Formation History

We derive the SFH from our constraints on the far-UV emissivity in a similar manner to galaxy surveys that measure the rest-frame UV emission (*5, 6, 31, 90, 91*). The conversion into star-formation rate (SFR) requires two assumptions: i) the amount of UV emission expected per unit SFR, $\mathscr{K}_{\rm UV}$, which is dictated by the initial mass function (IMF) of choice, and ii) the mean dust extinction within the host galaxies, A_V, since photons become a part of the EBL only if they escape their progenitor galaxies. For the former quantity, we assume $\mathscr{K}_{\rm UV} = 7.25 \times 10^{-29} {\rm M}_\odot \ {\rm yr}^{-1} \ {\rm erg}^{-1} \ {\rm s \ Hz}$ which is consistent with a Chabrier IMF (*92*). Our results on the SFH can be re-scaled by constant factor of 1.6 to represent a Salpeter IMF (*93*).

For the dust extinction correction, we rely on measured values of the mean A_V from the literature and fit its evolution with redshift using the following parametrization: $A_V \propto \frac{(1+z)^f}{1+\left(\frac{1+z}{c}\right)^d}$. The result is shown in Figure S10. The measured values of A_V are based on different methods. For instance, these come from: measured UV continuum slopes (*90, 94*), stellar population synthesis SED fitting (*10, 95*) and comparison of the integrated UV and IR luminosity functions (*28, 96*). We choose to use only those data that are measured from a large sample where robust uncertainty estimation is provided. Studies that assume or estimate values of A_V do not contribute to the fit but are shown in Figure S10 for reference. We obtain the evolving extinction:

$$A_V(z) = (1.49 \pm 0.07) \frac{(1+z)^{(0.64 \pm 0.19)}}{1 + [(1+z)/(3.40 \pm 0.44)]^{(3.54 \pm 0.47)}}. \quad \text{(S14)}$$

The SFH is then calculated as:

$$\rho_\star(z) = j_{\rm UV}(z) \cdot \mathscr{K}_{\rm UV} \cdot 10^{0.4 A_V} \quad \text{(S15)}$$

where $j_{\rm UV}(z)$ is our reconstructed emissivity at 1600Å.

The confidence regions for the cosmic SFH are shown in Figure 3 in the main paper along with data points from UV-derived measurements (*1*). We also display the same result in Figure S11 showing data from various studies using different tracers of SFR, including limits from γ-ray constraints of the EBL (*103*). At low and intermediate redshifts, our results are in good agreement with (albeit a little bit above) independent measurements from galaxy surveys. At $z > 3$, our results are in agreement, within the uncertainties, but favor a rather low SFH. As discussed in the previous subsection, this is primarily driven by GRB 080916C. More importantly, because the SFH derived from γ-ray absorption complements traditional methods that probe the SFH from sources resolved in surveys, our results imply that the bulk of star formation across cosmic time is already accounted for by surveys.

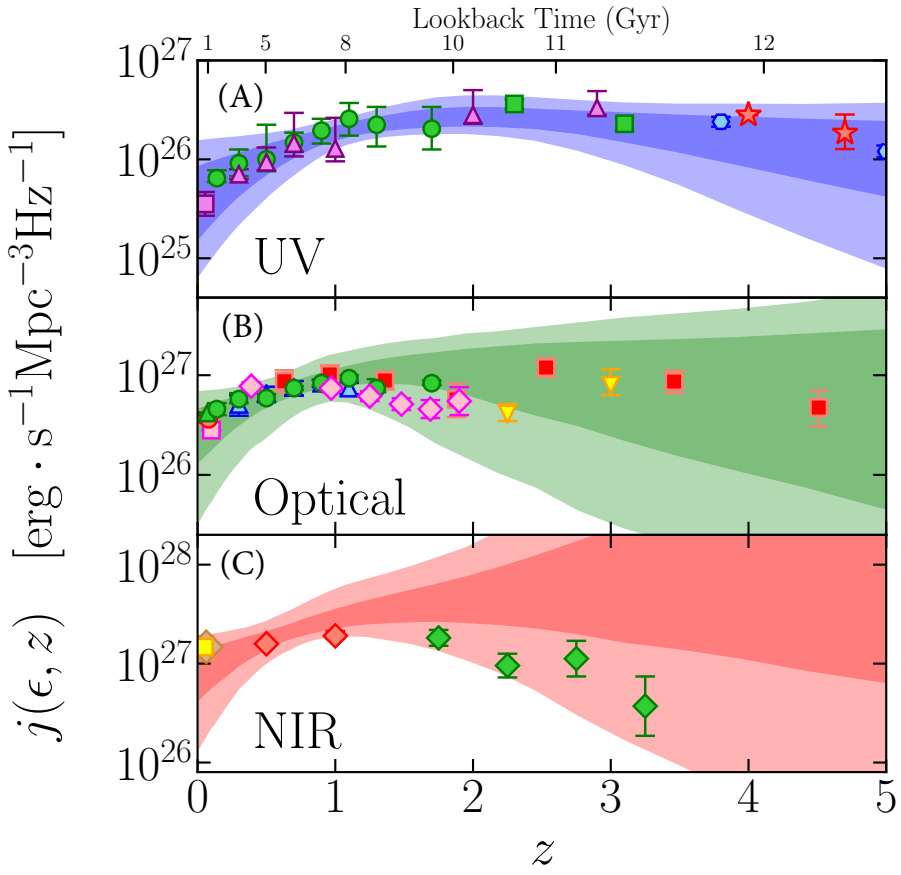

Figure S9 **Evolution of the cosmic emissivity.** The evolution of the cosmic emissivity at UV (0.16 µm), optical (0.45 µm) and NIR (1.6 µm), panels A, B and C respectively. The shaded regions show the 1σ and 2σ confidence regions resulting from the empirical EBL reconstruction model. The data points shown have rest-frame wavelengths in the range 0.15-0.17µm, 0.42-0.48µm and 1.25-1.27µm in the UV, optical, and NIR panels respectively. Colors and symbols follow the same scheme as in Figure S7.

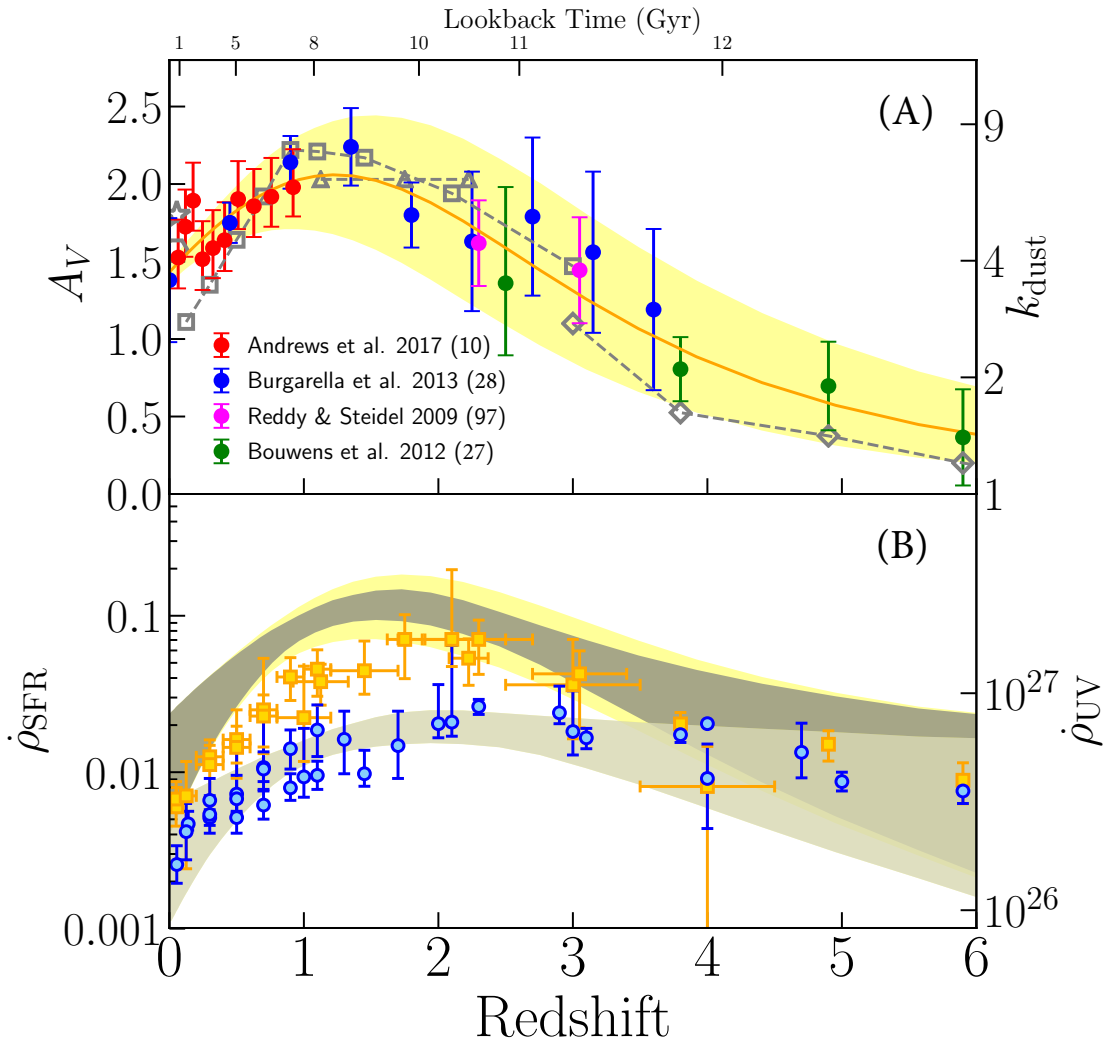

Figure S10 **The effects of dust extinction on the derived SFH**. *Panel A:* The mean dust extinction as a function of redshift. The solid line is our best fit (see Equation S14) with uncertainty shown as yellow region. Data points used for the fit (filled circles) are from (*10, 27, 28, 97*). Also shown as gray connected points are estimates from other references without published uncertainties: (*98*) star, (*99*) hexagon, (*100*) triangles, (*95*) squares, (*94*) diamonds. Right vertical axis shows the multiplicative factor $k_{\rm dust} = 10^{0.4A_V}$. *Panel B:* The SFH corrected (dark gray) and uncorrected (light gray) for dust extinction (in $\rm M_\odot\ yr^{-1}Mpc^{-3}$). Yellow region includes the systematic uncertainty from the dust correction which has been added in quadrature to the statistical uncertainties. The data points show the corrected (orange) and uncorrected (blue) SFH from the compilation of (*1*) with the addition of (*101*) and (*102*). Right vertical axis shows the UV emissivity in units of $\rm erg\ s^{-1}Mpc^{-3}Hz^{-1}$.

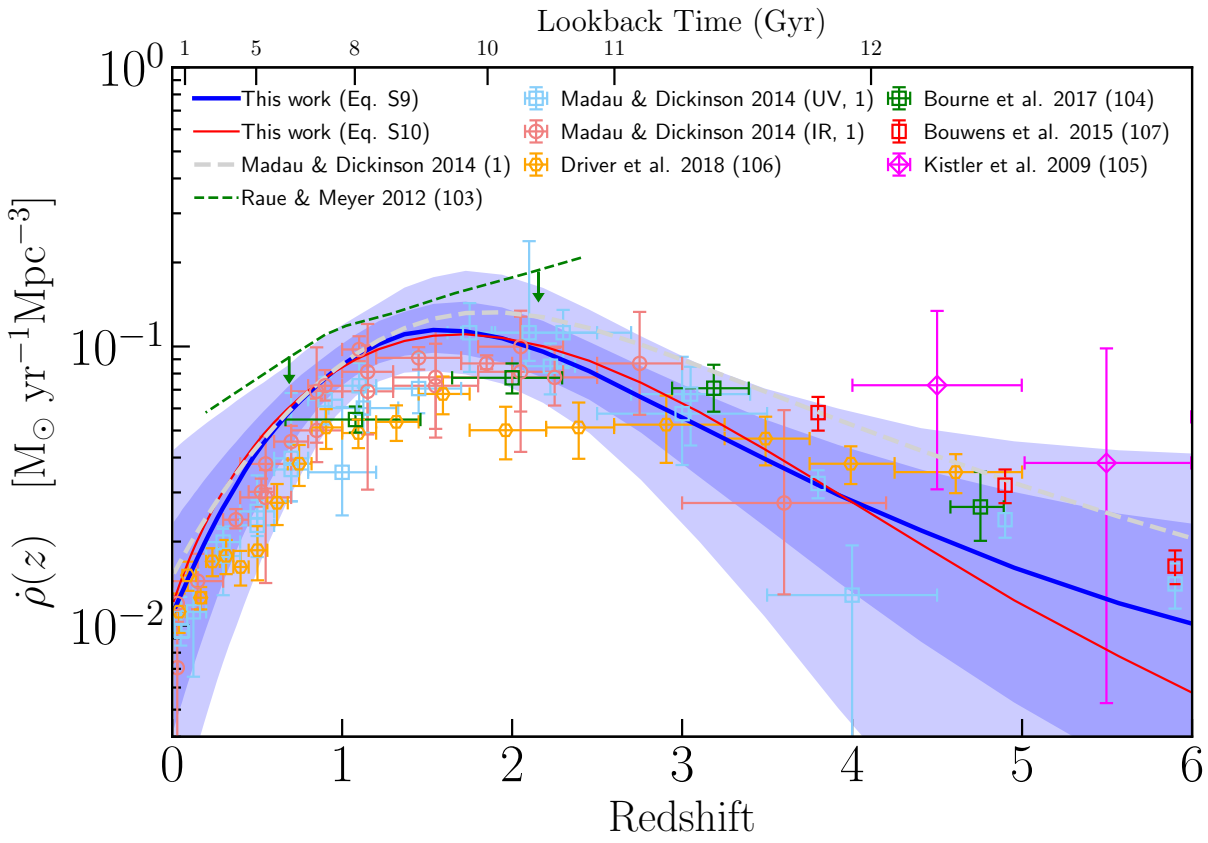

Figure S11 **The star-formation history of the Universe.** Results for the SFH compared with data from the literature. The blue and red lines compare the median SFH resulting from our EBL reconstruction using the evolution parameterization in Eq. S9 from (*1*) versus the parametrization in Eq. S10 from (*73*). The blue regions show the 1σ and 2σ confidence intervals for the EBL reconstruction model. The dashed gray line shows the fit from (*1*) and dashed green line are upper limits from γ-ray data derived by (*103*) where they assume a Chabrier IMF and $\beta = 0.3$. Data points are from the compilation of (*1*) with the addition of data from (*104–107*). The data have been corrected for variations in the adopted IMF to $\mathscr{K}_{\rm UV} = 7.25 \times 10^{-29}$ consistent with a Chabrier IMF (see text).

Stellar Population Model Method

The cosmic SFH, $\dot{\rho}(z)$, is the starting point in the EBL model of (*29, 108*) making it a useful model for further exploration of the parameter space that is made possible by the γ-ray optical

depth data. The model assumes that stars emit as blackbodies, with their temperatures, luminosities, and time evolution determined from formulae given by (*109*). The radiation emitted by stars is convolved with an IMF and star-formation rate density parameterization to get the luminosity density $j(\epsilon; z)$. The fraction of light that escapes dust extinction ($f_{\rm esc,dust}$) is based on the extinction curve from (*110*), which was derived from a fit to the luminosity density data in the local Universe. We let the dust extinction evolve according to Equation S14. The infrared portion of the EBL is computed assuming that all the energy absorbed by dust is re-radiated in the infrared. The SFH and IMF model parameters were chosen to reproduce the luminosity density data available at the time. Once $j(\epsilon; z)$ is calculated, the EBL number density and γ-ray absorption optical depth are computed from Equations S5–S7 above.

Using the methodology of (*29*), we have performed an MCMC fit to the γ-ray optical depth data. We parameterize the SFH and let the parameters vary, calculating the resulting EBL and optical depths in each step. A similar MCMC model fit, but limited to $z \geq 2$, was done by (*111*) to the earlier EBL absorption data from (*13*). We use the standard parameterization for the SFH (Equation S9), but also consider evolution according to Equation S10. The SFH result from our MCMC fits, reported in Figure 3 (as the green confidence region), are consistent with the SFH used for the "model C" of (*29*), which relied on the (*73*) parametrization with free parameters given by (*112*), at all values of z, but the confidence interval is particularly narrow up to $z \leq 2.5$. Table S5 reports the values of the SFH obtained from both methods as displayed in Figure 3.

The contribution of Active Galactic Nuclei

The methods employed here to derive the SFH of the Universe rest on the assumption that most of the EBL is the product of stellar emission. While this is almost certainly true in the IR and optical bands, there could be a non-negligible contribution of active galactic nuclei (AGN) to the global UV background (*37*). We estimate this contribution by considering measurements of the integrated quasar luminosity function. A fitting formula for the resulting emissivity as a function of redshift was provided by (*113*) at a rest-frame wavelength of 912Å. We convert this to 0.16 μm (the wavelength used to estimate our SFH) adopting the same power law spectrum $\propto \lambda^{-0.61}$ (*114*) and show the ratio of the AGN to total (as estimated in this work) emissivities at 0.16 μm in Figure S12. This shows that the contribution from known AGN is no more than a few percent. This is in agreement with the recent estimate of the AGN contribution to the EBL (*77*).

Table S5. The Cosmic star-formation history as reported in Figure 3, also available online.

z	Physical EBL model ($10^{-2}\mathrm{M}_\odot\ \mathrm{yr}^{-1}\ \mathrm{Mpc}^{-3}$)	EBL Reconstruction ($10^{-2}\mathrm{M}_\odot\ \mathrm{yr}^{-1}\ \mathrm{Mpc}^{-3}$)
0.0	$0.8^{+0.7}_{-0.3}$	$1.2^{+1.3}_{-0.7}$
0.1	$1.1^{+0.8}_{-0.4}$	$1.6^{+1.4}_{-0.9}$
0.2	$1.6^{+0.9}_{-0.5}$	$2.1^{+1.4}_{-1.1}$
0.3	$2.0^{+0.9}_{-0.5}$	$2.7^{+1.4}_{-1.2}$
0.4	$2.6^{+0.8}_{-0.6}$	$3.4^{+1.4}_{-1.4}$
0.5	$3.3^{+0.8}_{-0.6}$	$4.2^{+1.4}_{-1.5}$
0.6	$4.1^{+0.8}_{-0.7}$	$5.0^{+1.4}_{-1.5}$
0.8	$6.0^{+1.0}_{-0.9}$	$6.8^{+1.5}_{-1.4}$
1.0	$8.2^{+1.6}_{-1.4}$	$8.5^{+1.6}_{-1.3}$
1.2	$10.7^{+2.0}_{-2.2}$	$10.0^{+2.1}_{-1.5}$
1.4	$12.9^{+2.5}_{-2.8}$	$11.0^{+2.3}_{-1.8}$
1.6	$14.5^{+2.3}_{-2.9}$	$11.3^{+2.9}_{-2.0}$
1.8	$15.0^{+2.3}_{-2.5}$	$11.0^{+3.1}_{-2.0}$
2.0	$14.7^{+2.4}_{-2.4}$	$10.4^{+3.0}_{-1.9}$
2.5	$11.6^{+3.2}_{-2.9}$	$7.9^{+2.2}_{-1.7}$
3.0	$7.6^{+3.3}_{-2.4}$	$5.6^{+1.8}_{-1.8}$
3.5	$4.8^{+2.6}_{-1.8}$	$4.0^{+1.5}_{-1.7}$
4.0	$3.1^{+2.0}_{-1.3}$	$2.8^{+1.5}_{-1.5}$
4.5	$2.0^{+1.6}_{-0.9}$	$2.1^{+1.4}_{-1.3}$
5.0	$1.3^{+1.3}_{-0.7}$	$1.6^{+1.4}_{-1.1}$
5.5	$0.9^{+1.1}_{-0.5}$	$1.2^{+1.3}_{-0.9}$
6.0	$0.6^{+1.0}_{-0.3}$	$1.0^{+1.3}_{-0.8}$

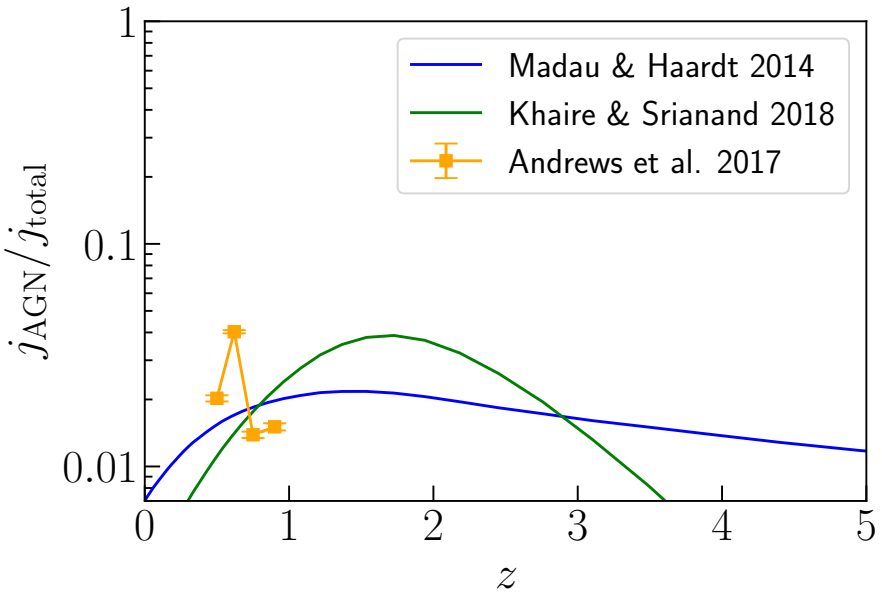

Figure S12 Ratio of emissivities of AGN vs total at 0.16 μm. The $j(\epsilon, z)_{\rm total}$ comes from the median UV emissivity derived from the optical depth data. The AGN emissivity is taken from the empirical fit of integrated quasar luminosity functions (converted to $0.16\mu{\rm m}$) provided by (*113*) and (*115*), plotted in blue and green respectively.

References and Notes

1. P. Madau, M. Dickinson, Cosmic Star-Formation History. *Annu. Rev. Astron. Astrophys.* **52**, 415–486 (2014). doi:10.1146/annurev-astro-081811-125615

2. N. A. Grogin, D. D. Kocevski, S. M. Faber, H. C. Ferguson, A. M. Koekemoer, A. G. Riess, V. Acquaviva, D. M. Alexander, O. Almaini, M. L. N. Ashby, M. Barden, E. F. Bell, F. Bournaud, T. M. Brown, K. I. Caputi, S. Casertano, P. Cassata, M. Castellano, P. Challis, R.-R. Chary, E. Cheung, M. Cirasuolo, C. J. Conselice, A. R. Cooray, D. J. Croton, E. Daddi, T. Dahlen, R. Davé, D. F. de Mello, A. Dekel, M. Dickinson, T. Dolch, J. L. Donley, J. S. Dunlop, A. A. Dutton, D. Elbaz, G. G. Fazio, A. V. Filippenko, S. L. Finkelstein, A. Fontana, J. P. Gardner, P. M. Garnavich, E. Gawiser, M. Giavalisco, A. Grazian, Y. Guo, N. P. Hathi, B. Häussler, P. F. Hopkins, J.-S. Huang, K.-H. Huang, S. W. Jha, J. S. Kartaltepe, R. P. Kirshner, D. C. Koo, K. Lai, K.-S. Lee, W. Li, J. M. Lotz, R. A. Lucas, P. Madau, P. J. McCarthy, E. J. McGrath, D. H. McIntosh, R. J. McLure, B. Mobasher, L. A. Moustakas, M. Mozena, K. Nandra, J. A. Newman, S.-M. Niemi, K. G. Noeske, C. J. Papovich, L. Pentericci, A. Pope, J. R. Primack, A. Rajan, S. Ravindranath, N. A. Reddy, A. Renzini, H.-W. Rix, A. R. Robaina, S. A. Rodney, D. J. Rosario, P. Rosati, S. Salimbeni, C. Scarlata, B. Siana, L. Simard, J. Smidt, R. S. Somerville, H. Spinrad, A. N. Straughn, L.-G. Strolger, O. Telford, H. I. Teplitz, J. R. Trump, A. van der Wel, C. Villforth, R. H. Wechsler, B. J. Weiner, T. Wiklind, V. Wild, G. Wilson, S. Wuyts, H.-J. Yan, M. S. Yun, CANDELS: The Cosmic Assembly Near-Infrared Deep Extragalactic Legacy Survey. *Astrophys. J. Suppl. Ser.* **197**, 35 (2011). doi:10.1088/0067-0049/197/2/35

3. G. D. Illingworth, D. Magee, P. A. Oesch, R. J. Bouwens, I. Labbé, M. Stiavelli, P. G. van Dokkum, M. Franx, M. Trenti, C. M. Carollo, V. Gonzalez, The *HST* Extreme Deep Field (XDF): Combining all ACS and WFC3/IR data on the HUDF region into the deepest field ever. *Astrophys. J. Suppl. Ser.* **209**, 6 (2013). doi:10.1088/0067-0049/209/1/6

4. J. M. Lotz, A. Koekemoer, D. Coe, N. Grogin, P. Capak, J. Mack, J. Anderson, R. Avila, E. A. Barker, D. Borncamp, G. Brammer, M. Durbin, H. Gunning, B. Hilbert, H. Jenkner, H. Khandrika, Z. Levay, R. A. Lucas, J. MacKenty, S. Ogaz, B. Porterfield, N. Reid, M. Robberto, P. Royle, L. J. Smith, L. J. Storrie-Lombardi, B. Sunnquist, J. Surace, D. C. Taylor, R. Williams, J. Bullock, M. Dickinson, S. Finkelstein, P. Natarajan, J. Richard, B. Robertson, J. Tumlinson, A. Zitrin, K. Flanagan, K. Sembach, B. T. Soifer, M. Mountain, The Frontier Fields: Survey Design and Initial Results. *Astrophys. J.* **837**, 97 (2017). doi:10.3847/1538-4357/837/1/97

5. R. J. McLure, J. S. Dunlop, R. A. A. Bowler, E. Curtis-Lake, M. Schenker, R. S. Ellis, B. E. Robertson, A. M. Koekemoer, A. B. Rogers, Y. Ono, M. Ouchi, S. Charlot, V. Wild, D. P. Stark, S. R. Furlanetto, M. Cirasuolo, T. A. Targett, A new multifield determination of the galaxy luminosity function at z = 7–9 incorporating the 2012 Hubble Ultra-Deep

Field imaging. *Mon. Not. R. Astron. Soc.* **432**, 2696–2716 (2013). doi:10.1093/mnras/stt627

6. D. Schiminovich, O. Ilbert, S. Arnouts, B. Milliard, L. Tresse, O. Le Fèvre, M. Treyer, T. K. Wyder, T. Budavári, E. Zucca, G. Zamorani, D. C. Martin, C. Adami, M. Arnaboldi, S. Bardelli, T. Barlow, L. Bianchi, M. Bolzonella, D. Bottini, Y.-I. Byun, A. Cappi, T. Contini, S. Charlot, J. Donas, K. Forster, S. Foucaud, P. Franzetti, P. G. Friedman, B. Garilli, I. Gavignaud, L. Guzzo, T. M. Heckman, C. Hoopes, A. Iovino, P. Jelinsky, V. Le Brun, Y.-W. Lee, D. Maccagni, B. F. Madore, R. Malina, B. Marano, C. Marinoni, H. J. McCracken, A. Mazure, B. Meneux, P. Morrissey, S. Neff, S. Paltani, R. Pellò, J. P. Picat, A. Pollo, L. Pozzetti, M. Radovich, R. M. Rich, R. Scaramella, M. Scodeggio, M. Seibert, O. Siegmund, T. Small, A. S. Szalay, G. Vettolani, B. Welsh, C. K. Xu, A. Zanichelli, The *GALEX*-VVDS Measurement of the Evolution of the Far-Ultraviolet Luminosity Density and the Cosmic Star Formation Rate. *Astrophys. J.* **619**, L47–L50 (2005). doi:10.1086/427077

7. M. G. Hauser, E. Dwek, The Cosmic Infrared Background: Measurements and Implications. *Annu. Rev. Astron. Astrophys.* **39**, 249–307 (2001). doi:10.1146/annurev.astro.39.1.249

8. A. Kashlinsky, Cosmic infrared background and early galaxy evolution. *Phys. Rep.* **409**, 361–438 (2005). doi:10.1016/j.physrep.2004.12.005

9. E. Dwek, F. Krennrich, The extragalactic background light and the gamma-ray opacity of the universe. *Astropart. Phys.* **43**, 112–133 (2013). doi:10.1016/j.astropartphys.2012.09.003

10. S. K. Andrews, S. P. Driver, L. J. M. Davies, P. R. Kafle, A. S. G. Robotham, K. Vinsen, A. H. Wright, J. Bland-Hawthorn, N. Bourne, M. Bremer, E. da Cunha, M. Drinkwater, B. Holwerda, A. M. Hopkins, L. S. Kelvin, J. Loveday, S. Phillipps, S. Wilkins, Galaxy and Mass Assembly: The evolution of the cosmic spectral energy distribution from z = 1 to z = 0. *Mon. Not. R. Astron. Soc.* **470**, 1342–1359 (2017). doi:10.1093/mnras/stx1279

11. A I. Nikishov, Absorption of High-Energy Photons in the Universe. *Sov. Phys. JETP* **14**, 393 (1962).

12. We adopted the following values for the Hubble constant and cosmological parameters: H_0 = 70 km s^{-1} Mpc^{-1}, $\Omega_M = 0.3$, and $\Omega_\Lambda = 0.7$.

13. M. Ackermann, M. Ajello, A. Allafort, P. Schady, L. Baldini, J. Ballet, G. Barbiellini, D. Bastieri, R. Bellazzini, R. D. Blandford, E. D. Bloom, A. W. Borgland, E. Bottacini, A. Bouvier, J. Bregeon, M. Brigida, P. Bruel, R. Buehler, S. Buson, G. A. Caliandro, R. A. Cameron, P. A. Caraveo, E. Cavazzuti, C. Cecchi, E. Charles, R. C. G. Chaves, A. Chekhtman, C. C. Cheung, J. Chiang, G. Chiaro, S. Ciprini, R. Claus, J. Cohen-Tanugi, J. Conrad, S. Cutini, F. D'Ammando, F. de Palma, C. D. Dermer, S. W. Digel, E. do Couto e Silva, A. Domínguez, P. S. Drell, A. Drlica-Wagner, C. Favuzzi, S. J. Fegan, W. B. Focke, A. Franckowiak, Y. Fukazawa, S. Funk, P. Fusco, F. Gargano, D. Gasparrini, N.

Gehrels, S. Germani, N. Giglietto, F. Giordano, M. Giroletti, T. Glanzman, G. Godfrey, I. A. Grenier, J. E. Grove, S. Guiriec, M. Gustafsson, D. Hadasch, M. Hayashida, E. Hays, M. S. Jackson, T. Jogler, J. Kataoka, J. Knödlseder, M. Kuss, J. Lande, S. Larsson, L. Latronico, F. Longo, F. Loparco, M. N. Lovellette, P. Lubrano, M. N. Mazziotta, J. E. McEnery, J. Mehault, P. F. Michelson, T. Mizuno, C. Monte, M. E. Monzani, A. Morselli, I. V. Moskalenko, S. Murgia, A. Tramacere, E. Nuss, J. Greiner, M. Ohno, T. Ohsugi, N. Omodei, M. Orienti, E. Orlando, J. F. Ormes, D. Paneque, J. S. Perkins, M. Pesce-Rollins, F. Piron, G. Pivato, T. A. Porter, S. Rainò, R. Rando, M. Razzano, S. Razzaque, A. Reimer, O. Reimer, L. C. Reyes, S. Ritz, A. Rau, C. Romoli, M. Roth, M. Sánchez-Conde, D. A. Sanchez, J. D. Scargle, C. Sgrò, E. J. Siskind, G. Spandre, P. Spinelli, Ł. Stawarz, D. J. Suson, H. Takahashi, T. Tanaka, J. G. Thayer, D. J. Thompson, L. Tibaldo, M. Tinivella, D. F. Torres, G. Tosti, E. Troja, T. L. Usher, J. Vandenbroucke, V. Vasileiou, G. Vianello, V. Vitale, A. P. Waite, B. L. Winer, K. S. Wood, M. Wood, The imprint of the extragalactic background light in the gamma-ray spectra of blazars. *Science* **338**, 1190–1192 (2012). doi:10.1126/science.1227160 Medline

14. See supplementary materials.

15. S. P. Driver, S. K. Andrews, L. J. Davies, A. S. G. Robotham, A. H. Wright, R. A. Windhorst, S. Cohen, K. Emig, R. A. Jansen, L. Dunne, Measurements of extragalactic background light from the far UV to the far IR from deep ground- and space-based galaxy counts. *Astrophys. J.* **827**, 108 (2016). doi:10.3847/0004-637X/827/2/108

16. J. P. Gardner, T. M. Brown, H. C. Ferguson, Ultraviolet Galaxy Counts from Space Telescope Imaging Spectrograph Observations of the Hubble Deep Fields. *Astrophys. J.* **542**, L79–L82 (2000). doi:10.1086/312930

17. C. K. Xu, J. Donas, S. Arnouts, T. K. Wyder, M. Seibert, J. Iglesias-Páramo, J. Blaizot, T. Small, B. Milliard, D. Schiminovich, D. C. Martin, T. A. Barlow, L. Bianchi, Y.-I. Byun, K. Forster, P. G. Friedman, T. M. Heckman, P. N. Jelinsky, Y.-W. Lee, B. F. Madore, R. F. Malina, P. Morrissey, S. G. Neff, R. M. Rich, O. H. W. Siegmund, A. S. Szalay, B. Y. Welsh, Number Counts of *GALEX* Sources in Far-Ultraviolet (1530 Å) and Near-Ultraviolet (2310 Å) Bands. *Astrophys. J.* **619**, L11–L14 (2005). doi:10.1086/425252

18. E. N. Voyer, J. P. Gardner, H. I. Teplitz, B. D. Siana, D. F. de Mello, Far-ultraviolet number counts of field galaxies. *Astrophys. J.* **736**, 80 (2011). doi:10.1088/0004-637X/736/2/80

19. R. C. Keenan, A. J. Barger, L. L. Cowie, W.-H. Wang, The resolved near-infrared extragalactic background. *Astrophys. J.* **723**, 40–46 (2010). doi:10.1088/0004-637X/723/1/40

20. M. L. N. Ashby, S. A. Stanford, M. Brodwin, A. H. Gonzalez, J. Martinez-Manso, J. G. Bartlett, B. A. Benson, L. E. Bleem, T. M. Crawford, A. Dey, A. Dressler, P. R. M. Eisenhardt, A. Galametz, B. T. Jannuzi, D. P. Marrone, S. Mei, A. Muzzin, F. Pacaud, M. Pierre, D. Stern, J. D. Vieira, The *Spitzer* South Pole Telescope deep field: Survey design

and infrared array camera catalogs. *Astrophys. J. Suppl. Ser.* **209**, 22 (2013). doi:10.1088/0067-0049/209/2/22

21. R. A. Bernstein, The Optical Extragalactic Background Light: Revisions and Further Comments. *Astrophys. J.* **666**, 663–673 (2007). doi:10.1086/519824

22. S. Matsuura, T. Arai, J. J. Bock, A. Cooray, P. M. Korngut, M. G. Kim, H. M. Lee, D. H. Lee, L. R. Levenson, T. Matsumoto, Y. Onishi, M. Shirahata, K. Tsumura, T. Wada, M. Zemcov, New Spectral Evidence of an Unaccounted Component of the Near-infrared Extragalactic Background Light from the *CIBER*. *Astrophys. J.* **839**, 7 (2017). doi:10.3847/1538-4357/aa6843

23. M. Zemcov, J. Smidt, T. Arai, J. Bock, A. Cooray, Y. Gong, M. G. Kim, P. Korngut, A. Lam, D. H. Lee, T. Matsumoto, S. Matsuura, U. W. Nam, G. Roudier, K. Tsumura, T. Wada, On the origin of near-infrared extragalactic background light anisotropy. *Science* **346**, 732–735 (2014). doi:10.1126/science.1258168 Medline

24. C. Burke, M. Hilton, C. Collins, Coevolution of brightest cluster galaxies and intracluster light using CLASH. *Mon. Not. R. Astron. Soc.* **449**, 2353–2367 (2015). doi:10.1093/mnras/stv450

25. The contribution of active galactic nuclei is small in comparison (*14*).

26. R. C. Kennicutt Jr., Star formation in galaxies along the Hubble sequence. *Annu. Rev. Astron. Astrophys.* **36**, 189–231 (1998). doi:10.1146/annurev.astro.36.1.189

27. R. J. Bouwens, G. D. Illingworth, P. A. Oesch, M. Franx, I. Labbé, M. Trenti, P. van Dokkum, C. M. Carollo, V. González, R. Smit, D. Magee, UV-continuum slopes at $z \sim$ 4-7 from the HUDF09+ERS+CANDELS observations: Discovery of a well-defined UV color-magnitude relationship for $z \geqslant 4$ star-forming galaxies. *Astrophys. J.* **754**, 83 (2012). doi:10.1088/0004-637X/754/2/83

28. D. Burgarella, V. Buat, C. Gruppioni, O. Cucciati, S. Heinis, S. Berta, M. Béthermin, J. Bock, A. Cooray, J. S. Dunlop, D. Farrah, A. Franceschini, E. Le Floc'h, D. Lutz, B. Magnelli, R. Nordon, S. J. Oliver, M. J. Page, P. Popesso, F. Pozzi, L. Riguccini, M. Vaccari, M. Viero, *Herschel* PEP/HerMES: The redshift evolution ($0 \leq z \leq 4$) of dust attenuation and of the total (UV+IR) star formation rate density. *Astron. Astrophys.* **554**, A70 (2013). doi:10.1051/0004-6361/201321651

29. J. D. Finke, S. Razzaque, C. D. Dermer, Modeling the extragalactic background light from stars and dust. *Astrophys. J.* **712**, 238–249 (2010). doi:10.1088/0004-637X/712/1/238

30. Fermi LAT and Fermi GBM Collaborations, Fermi observations of high-energy gamma-ray emission from GRB 080916C. *Science* **323**, 1688–1693 (2009). doi:10.1126/science.1169101 Medline

31. S. L. Finkelstein, R. E. Ryan Jr., C. Papovich, M. Dickinson, M. Song, R. S. Somerville, H. C. Ferguson, B. Salmon, M. Giavalisco, A. M. Koekemoer, M. L. N. Ashby, P. Behroozi, M. Castellano, J. S. Dunlop, S. M. Faber, G. G. Fazio, A. Fontana, N. A. Grogin, N. Hathi, J. Jaacks, D. D. Kocevski, R. Livermore, R. J. McLure, E. Merlin, B. Mobasher, J. A. Newman, M. Rafelski, V. Tilvi, S. P. Willner, The evolution of the galaxy rest-frame ultraviolet luminosity function over the first two billion years. *Astrophys. J.* **810**, 71 (2015). doi:10.1088/0004-637X/810/1/71

32. B. E. Robertson, R. S. Ellis, S. R. Furlanetto, J. S. Dunlop, Cosmic reionization and early star-forming galaxies: A joint analysis of new constraints from Planck and the *Hubble Space Telescope*. *Astrophys. J.* **802**, L19 (2015). doi:10.1088/2041-8205/802/2/L19

33. R. C. Livermore, S. L. Finkelstein, J. M. Lotz, Directly Observing the Galaxies Likely Responsible for Reionization. *Astrophys. J.* **835**, 113 (2017). doi:10.3847/1538-4357/835/2/113

34. M. Ishigaki, R. Kawamata, M. Ouchi, M. Oguri, K. Shimasaku, Y. Ono, Full-data Results of *Hubble* Frontier Fields: UV Luminosity Functions at $z \sim 6$–10 and a Consistent Picture of Cosmic Reionization. *Astrophys. J.* **854**, 73 (2018). doi:10.3847/1538-4357/aaa544

35. R. J. Bouwens, P. A. Oesch, G. D. Illingworth, R. S. Ellis, M. Stefanon, The $z \sim 6$ Luminosity Function Fainter than −15 mag from the Hubble Frontier Fields: The Impact of Magnification Uncertainties. *Astrophys. J.* **843**, 129 (2017). doi:10.3847/1538-4357/aa70a4

36. H. Atek, J. Richard, J.-P. Kneib, D. Schaerer, The Extreme Faint End of the UV Luminosity Function at z∼6 Through Gravitational Telescopes: A comprehensive assessment of strong lensing uncertainties. arXiv:1803.09747 (26 March 2018).

37. A. Domínguez, J. R. Primack, D. J. Rosario, F. Prada, R. C. Gilmore, S. M. Faber, D. C. Koo, R. S. Somerville, M. A. Pérez-Torres, P. Pérez-González, J.-S. Huang, M. Davis, P. Guhathakurta, P. Barmby, C. J. Conselice, M. Lozano, J. A. Newman, M. C. Cooper, Extragalactic background light inferred from AEGIS galaxy-SED-type fractions. *Mon. Not. R. Astron. Soc.* **410**, 2556–2578 (2011). doi:10.1111/j.1365-2966.2010.17631.x

38. K. Helgason, A. Kashlinsky, Reconstructing the γ-ray photon optical depth of the Universe to $z \sim 4$ from multiwavelength galaxy survey data. *Astrophys. J.* **758**, L13 (2012). doi:10.1088/2041-8205/758/1/L13

39. A. Abramowski, F. Acero, F. Aharonian, A. G. Akhperjanian, G. Anton, S. Balenderan, A. Balzer, A. Barnacka, Y. Becherini, J. Becker Tjus, K. Bernlöhr, E. Birsin, J. Biteau, A. Bochow, C. Boisson, J. Bolmont, P. Bordas, J. Brucker, F. Brun, P. Brun, T. Bulik, S. Carrigan, S. Casanova, M. Cerruti, P. M. Chadwick, A. Charbonnier, R. C. G. Chaves, A. Cheesebrough, G. Cologna, J. Conrad, C. Couturier, M. Dalton, M. K. Daniel, I. D. Davids, B. Degrange, C. Deil, P. deWilt, H. J. Dickinson, A. Djannati-Ataï, W.

Domainko, L. O. C. Drury, G. Dubus, K. Dutson, J. Dyks, M. Dyrda, K. Egberts, P. Eger, P. Espigat, L. Fallon, C. Farnier, S. Fegan, F. Feinstein, M. V. Fernandes, D. Fernandez, A. Fiasson, G. Fontaine, A. Förster, M. Füßling, M. Gajdus, Y. A. Gallant, T. Garrigoux, H. Gast, B. Giebels, J. F. Glicenstein, B. Glück, D. Göring, M.-H. Grondin, S. Häffner, J. D. Hague, J. Hahn, D. Hampf, J. Harris, S. Heinz, G. Heinzelmann, G. Henri, G. Hermann, A. Hillert, J. A. Hinton, W. Hofmann, P. Hofverberg, M. Holler, D. Horns, A. Jacholkowska, C. Jahn, M. Jamrozy, I. Jung, M. A. Kastendieck, K. Katarzyński, U. Katz, S. Kaufmann, B. Khélifi, D. Klochkov, W. Kluźniak, T. Kneiske, N. Komin, K. Kosack, R. Kossakowski, F. Krayzel, H. Laffon, G. Lamanna, J.-P. Lenain, D. Lennarz, T. Lohse, A. Lopatin, C.-C. Lu, V. Marandon, A. Marcowith, J. Masbou, G. Maurin, N. Maxted, M. Mayer, T. J. L. McComb, M. C. Medina, J. Méhault, U. Menzler, R. Moderski, M. Mohamed, E. Moulin, C. L. Naumann, M. Naumann-Godo, M. de Naurois, D. Nedbal, N. Nguyen, J. Niemiec, S. J. Nolan, S. Ohm, E. de Oña Wilhelmi, B. Opitz, M. Ostrowski, I. Oya, M. Panter, D. Parsons, M. Paz Arribas, N. W. Pekeur, G. Pelletier, J. Perez, P.-O. Petrucci, B. Peyaud, S. Pita, G. Pühlhofer, M. Punch, A. Quirrenbach, M. Raue, A. Reimer, O. Reimer, M. Renaud, R. de los Reyes, F. Rieger, J. Ripken, L. Rob, S. Rosier-Lees, G. Rowell, B. Rudak, C. B. Rulten, V. Sahakian, D. A. Sanchez, A. Santangelo, R. Schlickeiser, A. Schulz, U. Schwanke, S. Schwarzburg, S. Schwemmer, F. Sheidaei, J. L. Skilton, H. Sol, G. Spengler, Ł. Stawarz, R. Steenkamp, C. Stegmann, F. Stinzing, K. Stycz, I. Sushch, A. Szostek, J.-P. Tavernet, R. Terrier, M. Tluczykont, K. Valerius, C. van Eldik, G. Vasileiadis, C. Venter, A. Viana, P. Vincent, H. J. Völk, F. Volpe, S. Vorobiov, M. Vorster, S. J. Wagner, M. Ward, R. White, A. Wierzcholska, D. Wouters, M. Zacharias, A. Zajczyk, A. A. Zdziarski, A. Zech, H.-S. Zechlin, Measurement of the extragalactic background light imprint on the spectra of the brightest blazars observed with H.E.S.S. *Astron. Astrophys.* **550**, A4 (2013). doi:10.1051/0004-6361/201220355

40. J. Biteau, D. A. Williams, The extragalactic background light, the Hubble constant, and anomalies: Conclusions from 20 years of TeV gamma-ray observations. *Astrophys. J.* **812**, 60 (2015). doi:10.1088/0004-637X/812/1/60

41. H. Abdalla, A. Abramowski, F. Aharonian, F. Ait Benkhali, A. G. Akhperjanian, T. Andersson, E. O. Angüner, M. Arakawa, M. Arrieta, P. Aubert, M. Backes, A. Balzer, M. Barnard, Y. Becherini, J. B. Tjus, D. Berge, S. Bernhard, K. Bernlöhr, R. Blackwell, M. Böttcher, C. Boisson, J. Bolmont, S. Bonnefoy, P. Bordas, J. Bregeon, F. Brun, P. Brun, M. Bryan, M. Büchele, T. Bulik, M. Capasso, J. Carr, S. Casanova, M. Cerruti, N. Chakraborty, R. C. G. Chaves, A. Chen, J. Chevalier, M. Coffaro, S. Colafrancesco, G. Cologna, B. Condon, J. Conrad, Y. Cui, I. D. Davids, J. Decock, B. Degrange, C. Deil, J. Devin, P. de Wilt, L. Dirson, A. Djannati-Ataï, W. Domainko, A. Donath, L. O. C. Drury, K. Dutson, J. Dyks, T. Edwards, K. Egberts, P. Eger, J.-P. Ernenwein, S. Eschbach, C. Farnier, S. Fegan, M. V. Fernandes, A. Fiasson, G. Fontaine, A. Förster, S. Funk, M. Füßling, S. Gabici, Y. A. Gallant, T. Garrigoux, G. Giavitto, B. Giebels, J. F. Glicenstein,

D. Gottschall, A. Goyal, M.-H. Grondin, J. Hahn, M. Haupt, J. Hawkes, G. Heinzelmann, G. Henri, G. Hermann, J. A. Hinton, W. Hofmann, C. Hoischen, T. L. Holch, M. Holler, D. Horns, A. Ivascenko, H. Iwasaki, A. Jacholkowska, M. Jamrozy, M. Janiak, D. Jankowsky, F. Jankowsky, M. Jingo, T. Jogler, L. Jouvin, I. Jung-Richardt, M. A. Kastendieck, K. Katarzyński, M. Katsuragawa, U. Katz, D. Kerszberg, D. Khangulyan, B. Khélifi, J. King, S. Klepser, D. Klochkov, W. Kluźniak, D. Kolitzus, N. Komin, K. Kosack, S. Krakau, M. Kraus, P. P. Krüger, H. Laffon, G. Lamanna, J. Lau, J.-P. Lees, J. Lefaucheur, V. Lefranc, A. Lemière, M. Lemoine-Goumard, J.-P. Lenain, E. Leser, T. Lohse, M. Lorentz, R. Liu, R. López-Coto, I. Lypova, V. Marandon, A. Marcowith, C. Mariaud, R. Marx, G. Maurin, N. Maxted, M. Mayer, P. J. Meintjes, M. Meyer, A. M. W. Mitchell, R. Moderski, M. Mohamed, L. Mohrmann, K. Morå, E. Moulin, T. Murach, S. Nakashima, M. de Naurois, F. Niederwanger, J. Niemiec, L. Oakes, P. O'Brien, H. Odaka, S. Ohm, M. Ostrowski, I. Oya, M. Padovani, M. Panter, R. D. Parsons, N. W. Pekeur, G. Pelletier, C. Perennes, P.-O. Petrucci, B. Peyaud, Q. Piel, S. Pita, H. Poon, D. Prokhorov, H. Prokoph, G. Pühlhofer, M. Punch, A. Quirrenbach, S. Raab, R. Rauth, A. Reimer, O. Reimer, M. Renaud, R. de los Reyes, S. Richter, F. Rieger, C. Romoli, G. Rowell, B. Rudak, C. B. Rulten, V. Sahakian, S. Saito, D. Salek, D. A. Sanchez, A. Santangelo, M. Sasaki, R. Schlickeiser, F. Schüssler, A. Schulz, U. Schwanke, S. Schwemmer, M. Seglar-Arroyo, M. Settimo, A. S. Seyffert, N. Shafi, I. Shilon, R. Simoni, H. Sol, F. Spanier, G. Spengler, F. Spies, Ł. Stawarz, R. Steenkamp, C. Stegmann, K. Stycz, I. Sushch, T. Takahashi, J.-P. Tavernet, T. Tavernier, A. M. Taylor, R. Terrier, L. Tibaldo, D. Tiziani, M. Tluczykont, C. Trichard, N. Tsuji, R. Tuffs, Y. Uchiyama, D. J. van der Walt, C. van Eldik, C. van Rensburg, B. van Soelen, G. Vasileiadis, J. Veh, C. Venter, A. Viana, P. Vincent, J. Vink, F. Voisin, H. J. Völk, T. Vuillaume, Z. Wadiasingh, S. J. Wagner, P. Wagner, R. M. Wagner, R. White, A. Wierzcholska, P. Willmann, A. Wörnlein, D. Wouters, R. Yang, D. Zaborov, M. Zacharias, R. Zanin, A. A. Zdziarski, A. Zech, F. Zefi, A. Ziegler, N. Żywucka, Measurement of the EBL spectral energy distribution using the VHE γ-ray spectra of H.E.S.S. blazars. *Astron. Astrophys.* **606**, A59 (2017). doi:10.1051/0004-6361/201731200

42. M. Meyer, M. Raue, D. Mazin, D. Horns, Limits on the extragalactic background light in the *Fermi* era. *Astron. Astrophys.* **542**, A59 (2012). doi:10.1051/0004-6361/201118284

43. M. Ackermann, M. Ajello, W. B. Atwood, L. Baldini, J. Ballet, G. Barbiellini, D. Bastieri, J. B. Gonzalez, R. Bellazzini, E. Bissaldi, R. D. Blandford, E. D. Bloom, R. Bonino, E. Bottacini, T. J. Brandt, J. Bregeon, R. J. Britto, P. Bruel, R. Buehler, S. Buson, G. A. Caliandro, R. A. Cameron, M. Caragiulo, P. A. Caraveo, B. Carpenter, J. M. Casandjian, E. Cavazzuti, C. Cecchi, E. Charles, A. Chekhtman, C. C. Cheung, J. Chiang, G. Chiaro, S. Ciprini, R. Claus, J. Cohen-Tanugi, L. R. Cominsky, J. Conrad, S. Cutini, R. D'Abrusco, F. D'Ammando, A. Angelis, R. Desiante, S. W. Digel, L. D. Venere, P. S. Drell, C. Favuzzi, S. J. Fegan, E. C. Ferrara, J. Finke, W. B. Focke, A. Franckowiak, L.

Fuhrmann, Y. Fukazawa, A. K. Furniss, P. Fusco, F. Gargano, D. Gasparrini, N. Giglietto, P. Giommi, F. Giordano, M. Giroletti, T. Glanzman, G. Godfrey, I. A. Grenier, J. E. Grove, S. Guiriec, J. W. Hewitt, A. B. Hill, D. Horan, R. Itoh, G. Jóhannesson, A. S. Johnson, W. N. Johnson, J. Kataoka, T. Kawano, F. Krauss, M. Kuss, G. L. Mura, S. Larsson, L. Latronico, C. Leto, J. Li, L. Li, F. Longo, F. Loparco, B. Lott, M. N. Lovellette, P. Lubrano, G. M. Madejski, M. Mayer, M. N. Mazziotta, J. E. McEnery, P. F. Michelson, T. Mizuno, A. A. Moiseev, M. E. Monzani, A. Morselli, I. V. Moskalenko, S. Murgia, E. Nuss, M. Ohno, T. Ohsugi, R. Ojha, N. Omodei, M. Orienti, E. Orlando, A. Paggi, D. Paneque, J. S. Perkins, M. Pesce-Rollins, F. Piron, G. Pivato, T. A. Porter, S. Rainò, R. Rando, M. Razzano, S. Razzaque, A. Reimer, O. Reimer, R. W. Romani, D. Salvetti, M. Schaal, F. K. Schinzel, A. Schulz, C. Sgrò, E. J. Siskind, K. V. Sokolovsky, F. Spada, G. Spandre, P. Spinelli, L. Stawarz, D. J. Suson, H. Takahashi, T. Takahashi, Y. Tanaka, J. G. Thayer, J. B. Thayer, L. Tibaldo, D. F. Torres, E. Torresi, G. Tosti, E. Troja, Y. Uchiyama, G. Vianello, B. L. Winer, K. S. Wood, S. Zimmer, The third catalog of active galactic nuclei detected by the *FERMI* Large Area Telescope. *Astrophys. J.* **810**, 14 (2015). doi:10.1088/0004-637X/810/1/14

44. M. S. Shaw, R. W. Romani, G. Cotter, S. E. Healey, P. F. Michelson, A. C. S. Readhead, J. L. Richards, W. Max-Moerbeck, O. G. King, W. J. Potter, Spectroscopy of the largest ever γ-ray-selected BL LAC sample. *Astrophys. J.* **764**, 135 (2013). doi:10.1088/0004-637X/764/2/135

45. F. Acero, M. Ackermann, M. Ajello, A. Albert, L. Baldini, J. Ballet, G. Barbiellini, D. Bastieri, R. Bellazzini, E. Bissaldi, E. D. Bloom, R. Bonino, E. Bottacini, T. J. Brandt, J. Bregeon, P. Bruel, R. Buehler, S. Buson, G. A. Caliandro, R. A. Cameron, M. Caragiulo, P. A. Caraveo, J. M. Casandjian, E. Cavazzuti, C. Cecchi, E. Charles, A. Chekhtman, J. Chiang, G. Chiaro, S. Ciprini, R. Claus, J. Cohen-Tanugi, J. Conrad, A. Cuoco, S. Cutini, F. D'Ammando, A. Angelis, F. Palma, R. Desiante, S. W. Digel, L. D. Venere, P. S. Drell, C. Favuzzi, S. J. Fegan, E. C. Ferrara, W. B. Focke, A. Franckowiak, S. Funk, P. Fusco, F. Gargano, D. Gasparrini, N. Giglietto, F. Giordano, M. Giroletti, T. Glanzman, G. Godfrey, I. A. Grenier, S. Guiriec, D. Hadasch, A. K. Harding, K. Hayashi, E. Hays, J. W. Hewitt, A. B. Hill, D. Horan, X. Hou, T. Jogler, G. Jóhannesson, T. Kamae, M. Kuss, D. Landriu, S. Larsson, L. Latronico, J. Li, L. Li, F. Longo, F. Loparco, M. N. Lovellette, P. Lubrano, S. Maldera, D. Malyshev, A. Manfreda, P. Martin, M. Mayer, M. N. Mazziotta, J. E. McEnery, P. F. Michelson, N. Mirabal, T. Mizuno, M. E. Monzani, A. Morselli, E. Nuss, T. Ohsugi, N. Omodei, M. Orienti, E. Orlando, J. F. Ormes, D. Paneque, M. Pesce-Rollins, F. Piron, G. Pivato, S. Rainò, R. Rando, M. Razzano, S. Razzaque, A. Reimer, O. Reimer, Q. Remy, N. Renault, M. Sánchez-Conde, M. Schaal, A. Schulz, C. Sgrò, E. J. Siskind, F. Spada, G. Spandre, P. Spinelli, A. W. Strong, D. J. Suson, H. Tajima, H. Takahashi, J. B. Thayer, D. J. Thompson, L. Tibaldo, M. Tinivella, D. F. Torres, G. Tosti, E. Troja, G. Vianello, M. Werner, K. S. Wood, M. Wood, G. Zaharijas, S. Zimmer, Development of the model of galactic interstellar emission for

standard point-source analysis of *FERMI* Large Area Telescope data. *Astrophys. J. Suppl. Ser.* **223**, 26 (2016). doi:10.3847/0067-0049/223/2/26

46. The templates used are gll_iem_v06.fits and iso_P8R2_SOURCE_V6_v06.txt, available at https://fermi.gsfc.nasa.gov/ssc/data/access/lat/BackgroundModels.html.

47. F. Acero, M. Ackermann, M. Ajello, A. Albert, W. B. Atwood, M. Axelsson, L. Baldini, J. Ballet, G. Barbiellini, D. Bastieri, A. Belfiore, R. Bellazzini, E. Bissaldi, R. D. Blandford, E. D. Bloom, J. R. Bogart, R. Bonino, E. Bottacini, J. Bregeon, R. J. Britto, P. Bruel, R. Buehler, T. H. Burnett, S. Buson, G. A. Caliandro, R. A. Cameron, R. Caputo, M. Caragiulo, P. A. Caraveo, J. M. Casandjian, E. Cavazzuti, E. Charles, R. C. G. Chaves, A. Chekhtman, C. C. Cheung, J. Chiang, G. Chiaro, S. Ciprini, R. Claus, J. C. Tanugi, L. R. Cominsky, J. Conrad, S. Cutini, F. D'Ammando, A. Angelis, M. DeKlotz, F. Palma, R. Desiante, S. W. Digel, L. D. Venere, P. S. Drell, R. Dubois, D. Dumora, C. Favuzzi, S. J. Fegan, E. C. Ferrara, J. Finke, A. Franckowiak, Y. Fukazawa, S. Funk, P. Fusco, F. Gargano, D. Gasparrini, B. Giebels, N. Giglietto, P. Giommi, F. Giordano, M. Giroletti, T. Glanzman, G. Godfrey, I. A. Grenier, M.-H. Grondin, J. E. Grove, L. Guillemot, S. Guiriec, D. Hadasch, A. K. Harding, E. Hays, J. W. Hewitt, A. B. Hill, D. Horan, G. Iafrate, T. Jogler, G. Jóhannesson, R. P. Johnson, A. S. Johnson, T. J. Johnson, W. N. Johnson, T. Kamae, J. Kataoka, J. Katsuta, M. Kuss, G. L. Mura, D. Landriu, S. Larsson, L. Latronico, M. L. Goumard, J. Li, L. Li, F. Longo, F. Loparco, B. Lott, M. N. Lovellette, P. Lubrano, G. M. Madejski, F. Massaro, M. Mayer, M. N. Mazziotta, J. E. McEnery, P. F. Michelson, N. Mirabal, T. Mizuno, A. A. Moiseev, M. Mongelli, M. E. Monzani, A. Morselli, I. V. Moskalenko, S. Murgia, E. Nuss, M. Ohno, T. Ohsugi, N. Omodei, M. Orienti, E. Orlando, J. F. Ormes, D. Paneque, J. H. Panetta, J. S. Perkins, M. P. Rollins, F. Piron, G. Pivato, T. A. Porter, J. L. Racusin, R. Rando, M. Razzano, S. Razzaque, A. Reimer, O. Reimer, T. Reposeur, L. S. Rochester, R. W. Romani, D. Salvetti, M. S. Conde, P. M. S. Parkinson, A. Schulz, E. J. Siskind, D. A. Smith, F. Spada, G. Spandre, P. Spinelli, T. E. Stephens, A. W. Strong, D. J. Suson, H. Takahashi, T. Takahashi, Y. Tanaka, J. G. Thayer, J. B. Thayer, D. J. Thompson, L. Tibaldo, O. Tibolla, D. F. Torres, E. Torresi, G. Tosti, E. Troja, B. V. Klaveren, G. Vianello, B. L. Winer, K. S. Wood, M. Wood, S. Zimmer, *FERMI* Large Area Telescope Third Source Catalog. *Astrophys. J. Suppl. Ser.* **218**, 23 (2015). doi:10.1088/0067-0049/218/2/23

48. M. Ajello, M. S. Shaw, R. W. Romani, C. D. Dermer, L. Costamante, O. G. King, W. Max-Moerbeck, A. Readhead, A. Reimer, J. L. Richards, M. Stevenson, The luminosity function of *FERMI*-detected flat-spectrum radio quasars. *Astrophys. J.* **751**, 108 (2012). doi:10.1088/0004-637X/751/2/108

49. S. T. Scully, M. A. Malkan, F. W. Stecker, An empirical determination of the intergalactic background light using near-infrared deep galaxy survey data out to 5 μm and the gamma-ray opacity of the universe. *Astrophys. J.* **784**, 138 (2014). doi:10.1088/0004-637X/784/2/138

50. T. M. Kneiske, T. Bretz, K. Mannheim, D. H. Hartmann, Implications of cosmological gamma-ray absorption. *Astron. Astrophys.* **413**, 807–815 (2004). doi:10.1051/0004-6361:20031542

51. R. C. Gilmore, R. S. Somerville, J. R. Primack, A. Domínguez, Semi-analytic modelling of the extragalactic background light and consequences for extragalactic gamma-ray spectra. *Mon. Not. R. Astron. Soc.* **422**, 3189–3207 (2012). doi:10.1111/j.1365-2966.2012.20841.x

52. A. Franceschini, G. Rodighiero, The extragalactic background light revisited and the cosmic photon-photon opacity. *Astron. Astrophys.* **603**, A34 (2017). doi:10.1051/0004-6361/201629684

53. R. C. Gilmore, P. Madau, J. R. Primack, R. S. Somerville, F. Haardt, GeV gamma-ray attenuation and the high-redshift UV background. *Mon. Not. R. Astron. Soc.* **399**, 1694–1708 (2009). doi:10.1111/j.1365-2966.2009.15392.x

54. Y. Inoue, S. Inoue, M. A. R. Kobayashi, R. Makiya, Y. Niino, T. Totani, Extragalactic background light from hierarchical galaxy formation: Gamma-ray attenuation up to the epoch of cosmic reionization and the first stars. *Astrophys. J.* **768**, 197 (2013). doi:10.1088/0004-637X/768/2/197

55. T. M. Kneiske, H. Dole, A lower-limit flux for the extragalactic background light. *Astron. Astrophys.* **515**, A19 (2010). doi:10.1051/0004-6361/200912000

56. G. G. Fazio, F. W. Stecker, Predicted high energy break in the isotropic gamma ray spectrum: A test of cosmological origin. *Nature* **226**, 135–136 (1970). doi:10.1038/226135a0 Medline

57. A. Domínguez, J. D. Finke, F. Prada, J. R. Primack, F. S. Kitaura, B. Siana, D. Paneque, Detection of the cosmic γ-ray horizon from multiwavelength observations of blazars. *Astrophys. J.* **770**, 77 (2013). doi:10.1088/0004-637X/770/1/77

58. J. Greiner, C. Clemens, T. Krühler, A. von Kienlin, A. Rau, R. Sari, D. B. Fox, N. Kawai, P. Afonso, M. Ajello, E. Berger, S. B. Cenko, A. Cucchiara, R. Filgas, S. Klose, A. Küpcü Yoldaş, G. G. Lichti, S. Löw, S. McBreen, T. Nagayama, A. Rossi, S. Sato, G. Szokoly, A. Yoldaş, X.-L. Zhang, The redshift and afterglow of the extremely energetic gamma-ray burst GRB 080916C. *Astron. Astrophys.* **498**, 89–94 (2009). doi:10.1051/0004-6361/200811571

59. R. C. Gilmore, Constraining the near-infrared background light from Population III stars using high-redshift gamma-ray sources. *Mon. Not. R. Astron. Soc.* **420**, 800–809 (2012). doi:10.1111/j.1365-2966.2011.20092.x

60. Y. Inoue, Y. T. Tanaka, G. M. Madejski, A. Domínguez, Upper bound on the first star formation history. *Astrophys. J.* **781**, L35 (2014). doi:10.1088/2041-8205/781/2/L35

61. W. B. Atwood, L. Baldini, J. Bregeon, P. Bruel, A. Chekhtman, J. Cohen-Tanugi, A. Drlica-Wagner, J. Granot, F. Longo, N. Omodei, M. Pesce-Rollins, S. Razzaque, L. S. Rochester, C. Sgrò, M. Tinivella, T. L. Usher, S. Zimmer, New *FERMI*-LAT event reconstruction reveals more high-energy gamma rays from gamma-ray bursts. *Astrophys. J.* **774**, 76 (2013). doi:10.1088/0004-637X/774/1/76

62. A. Desai, M. Ajello, N. Omodei, D. H. Hartmann, A. Domínguez, V. S. Paliya, K. Helgason, J. Finke, M. Meyer, Probing the EBL Evolution at High Redshift Using GRBs Detected with the *Fermi*-LAT. *Astrophys. J.* **850**, 73 (2017). doi:10.3847/1538-4357/aa917c

63. We used the templates gll_iem_v06.fits and iso_P8R2_TRANSIENT020_V6_v06.txt, available at https://fermi.gsfc.nasa.gov/ssc/data/access/lat/BackgroundModels.html.

64. A. Tramacere, P. Giommi, M. Perri, F. Verrecchia, G. Tosti, *Swift* observations of the very intense flaring activity of Mrk 421 during 2006. I. Phenomenological picture of electron acceleration and predictions for MeV/GeV emission. *Astron. Astrophys.* **501**, 879–898 (2009). doi:10.1051/0004-6361/200810865

65. A. Tramacere, E. Massaro, A. M. Taylor, Stochastic acceleration and the evolution of spectral distributions in synchro-self-Compton sources: A self-consistent modeling of blazars' flares. *Astrophys. J.* **739**, 66 (2011). doi:10.1088/0004-637X/739/2/66

66. M. Ajello, W. B. Atwood, L. Baldini, J. Ballet, G. Barbiellini, D. Bastieri, R. Bellazzini, E. Bissaldi, R. D. Blandford, E. D. Bloom, R. Bonino, J. Bregeon, R. J. Britto, P. Bruel, R. Buehler, S. Buson, R. A. Cameron, R. Caputo, M. Caragiulo, P. A. Caraveo, E. Cavazzuti, C. Cecchi, E. Charles, A. Chekhtman, C. C. Cheung, G. Chiaro, S. Ciprini, J. M. Cohen, D. Costantin, F. Costanza, A. Cuoco, S. Cutini, F. D'Ammando, F. de Palma, R. Desiante, S. W. Digel, N. Di Lalla, M. Di Mauro, L. Di Venere, A. Domínguez, P. S. Drell, D. Dumora, C. Favuzzi, S. J. Fegan, E. C. Ferrara, P. Fortin, A. Franckowiak, Y. Fukazawa, S. Funk, P. Fusco, F. Gargano, D. Gasparrini, N. Giglietto, P. Giommi, F. Giordano, M. Giroletti, T. Glanzman, D. Green, I. A. Grenier, M.-H. Grondin, J. E. Grove, L. Guillemot, S. Guiriec, A. K. Harding, E. Hays, J. W. Hewitt, D. Horan, G. Jóhannesson, S. Kensei, M. Kuss, G. La Mura, S. Larsson, L. Latronico, M. Lemoine-Goumard, J. Li, F. Longo, F. Loparco, B. Lott, P. Lubrano, J. D. Magill, S. Maldera, A. Manfreda, M. N. Mazziotta, J. E. McEnery, M. Meyer, P. F. Michelson, N. Mirabal, W. Mitthumsiri, T. Mizuno, A. A. Moiseev, M. E. Monzani, A. Morselli, I. V. Moskalenko, M. Negro, E. Nuss, T. Ohsugi, N. Omodei, M. Orienti, E. Orlando, M. Palatiello, V. S. Paliya, D. Paneque, J. S. Perkins, M. Persic, M. Pesce-Rollins, F. Piron, T. A. Porter, G. Principe, S. Rainò, R. Rando, M. Razzano, S. Razzaque, A. Reimer, O. Reimer, T. Reposeur, P. M. Saz Parkinson, C. Sgrò, D. Simone, E. J. Siskind, F. Spada, G. Spandre, P. Spinelli, L. Stawarz, D. J. Suson, M. Takahashi, D. Tak, J. G. Thayer, J. B. Thayer, D. J. Thompson, D. F. Torres, E. Torresi, E. Troja, G. Vianello, K. Wood, M. Wood, 3FHL: The Third Catalog of Hard *Fermi*-LAT Sources. *Astrophys. J. Suppl. Ser.* **232**, 18 (2017). doi:10.3847/1538-4365/aa8221

67. M. Ackermann, M. Ajello, A. Albert, A. Allafort, E. Antolini, L. Baldini, J. Ballet, G. Barbiellini, D. Bastieri, K. Bechtol, R. Bellazzini, R. D. Blandford, E. D. Bloom, E. Bonamente, E. Bottacini, A. Bouvier, T. J. Brandt, J. Bregeon, M. Brigida, P. Bruel, R. Buehler, S. Buson, G. A. Caliandro, R. A. Cameron, P. A. Caraveo, E. Cavazzuti, C. Cecchi, E. Charles, A. Chekhtman, C. C. Cheung, J. Chiang, G. Chiaro, S. Ciprini, R. Claus, J. Cohen-Tanugi, J. Conrad, S. Cutini, M. Dalton, F. D'Ammando, A. de Angelis, F. de Palma, C. D. Dermer, L. Di Venere, P. S. Drell, A. Drlica-Wagner, C. Favuzzi, S. J. Fegan, E. C. Ferrara, W. B. Focke, A. Franckowiak, Y. Fukazawa, S. Funk, P. Fusco, F. Gargano, D. Gasparrini, S. Germani, N. Giglietto, F. Giordano, M. Giroletti, T. Glanzman, G. Godfrey, I. A. Grenier, M.-H. Grondin, J. E. Grove, S. Guiriec, D. Hadasch, Y. Hanabata, A. K. Harding, M. Hayashida, E. Hays, J. Hewitt, A. B. Hill, D. Horan, X. Hou, R. E. Hughes, Y. Inoue, M. S. Jackson, T. Jogler, G. Jóhannesson, W. N. Johnson, T. Kamae, J. Kataoka, T. Kawano, J. Knödlseder, M. Kuss, J. Lande, S. Larsson, L. Latronico, M. Lemoine-Goumard, F. Longo, F. Loparco, B. Lott, M. N. Lovellette, P. Lubrano, M. Mayer, M. N. Mazziotta, J. E. McEnery, P. F. Michelson, W. Mitthumsiri, T. Mizuno, C. Monte, M. E. Monzani, A. Morselli, I. V. Moskalenko, S. Murgia, R. Nemmen, E. Nuss, T. Ohsugi, A. Okumura, N. Omodei, M. Orienti, E. Orlando, J. F. Ormes, D. Paneque, J. H. Panetta, J. S. Perkins, M. Pesce-Rollins, F. Piron, G. Pivato, T. A. Porter, S. Rainò, R. Rando, M. Razzano, A. Reimer, O. Reimer, C. Romoli, M. Roth, M. Sánchez-Conde, J. D. Scargle, A. Schulz, C. Sgrò, E. J. Siskind, G. Spandre, P. Spinelli, D. J. Suson, H. Takahashi, Y. Takeuchi, J. G. Thayer, J. B. Thayer, D. J. Thompson, L. Tibaldo, M. Tinivella, D. F. Torres, G. Tosti, E. Troja, V. Tronconi, T. L. Usher, J. Vandenbroucke, V. Vasileiou, G. Vianello, V. Vitale, B. L. Winer, K. S. Wood, M. Wood, Z. Yang, The *FERMI* all-sky variability analysis: A list of flaring gamma-ray sources and the search for transients in our galaxy. *Astrophys. J.* **771**, 57 (2013). doi:10.1088/0004-637X/771/1/57

68. S. Abdollahi, M. Ackermann, M. Ajello, A. Albert, L. Baldini, J. Ballet, G. Barbiellini, D. Bastieri, J. Becerra Gonzalez, R. Bellazzini, E. Bissaldi, R. D. Blandford, E. D. Bloom, R. Bonino, E. Bottacini, J. Bregeon, P. Bruel, R. Buehler, S. Buson, R. A. Cameron, M. Caragiulo, P. A. Caraveo, E. Cavazzuti, C. Cecchi, A. Chekhtman, C. C. Cheung, G. Chiaro, S. Ciprini, J. Conrad, D. Costantin, F. Costanza, S. Cutini, F. D'Ammando, F. Palma, A. Desai, R. Desiante, S. W. Digel, N. D. Lalla, M. D. Mauro, L. D. Venere, B. Donaggio, P. S. Drell, C. Favuzzi, S. J. Fegan, E. C. Ferrara, W. B. Focke, A. Franckowiak, Y. Fukazawa, S. Funk, P. Fusco, F. Gargano, D. Gasparrini, N. Giglietto, M. Giomi, F. Giordano, M. Giroletti, T. Glanzman, D. Green, I. A. Grenier, J. E. Grove, L. Guillemot, S. Guiriec, E. Hays, D. Horan, T. Jogler, G. Jóhannesson, A. S. Johnson, D. Kocevski, M. Kuss, G. L. Mura, S. Larsson, L. Latronico, J. Li, F. Longo, F. Loparco, M. N. Lovellette, P. Lubrano, J. D. Magill, S. Maldera, A. Manfreda, M. Mayer, M. N. Mazziotta, P. F. Michelson, W. Mitthumsiri, T. Mizuno, M. E. Monzani, A. Morselli, I. V. Moskalenko, M. Negro, E. Nuss, T. Ohsugi, N. Omodei, M. Orienti, E. Orlando, V. S.

Paliya, D. Paneque, J. S. Perkins, M. Persic, M. Pesce-Rollins, V. Petrosian, F. Piron, T. A. Porter, G. Principe, S. Rainò, R. Rando, M. Razzano, S. Razzaque, A. Reimer, O. Reimer, C. Sgrò, D. Simone, E. J. Siskind, F. Spada, G. Spandre, P. Spinelli, L. Stawarz, D. J. Suson, M. Takahashi, K. Tanaka, J. B. Thayer, D. J. Thompson, D. F. Torres, E. Torresi, G. Tosti, E. Troja, G. Vianello, K. S. Wood, The Second Catalog of Flaring Gamma-Ray Sources from the Fermi All-sky Variability Analysis. *Astrophys. J.* **846**, 34 (2017). doi:10.3847/1538-4357/aa8092

69. M. Ackermann, M. Ajello, A. Albert, A. Allafort, W. B. Atwood, M. Axelsson, L. Baldini, J. Ballet, G. Barbiellini, D. Bastieri, K. Bechtol, R. Bellazzini, E. Bissaldi, R. D. Blandford, E. D. Bloom, J. R. Bogart, E. Bonamente, A. W. Borgland, E. Bottacini, A. Bouvier, T. J. Brandt, J. Bregeon, M. Brigida, P. Bruel, R. Buehler, T. H. Burnett, S. Buson, G. A. Caliandro, R. A. Cameron, P. A. Caraveo, J. M. Casandjian, E. Cavazzuti, C. Cecchi, Ö. Çelik, E. Charles, R. C. G. Chaves, A. Chekhtman, C. C. Cheung, J. Chiang, S. Ciprini, R. Claus, J. Cohen-Tanugi, J. Conrad, R. Corbet, S. Cutini, F. D'Ammando, D. S. Davis, A. de Angelis, M. DeKlotz, F. de Palma, C. D. Dermer, S. W. Digel, E. do Couto e Silva, P. S. Drell, A. Drlica-Wagner, R. Dubois, C. Favuzzi, S. J. Fegan, E. C. Ferrara, W. B. Focke, P. Fortin, Y. Fukazawa, S. Funk, P. Fusco, F. Gargano, D. Gasparrini, N. Gehrels, B. Giebels, N. Giglietto, F. Giordano, M. Giroletti, T. Glanzman, G. Godfrey, I. A. Grenier, J. E. Grove, S. Guiriec, D. Hadasch, M. Hayashida, E. Hays, D. Horan, X. Hou, R. E. Hughes, M. S. Jackson, T. Jogler, G. Jóhannesson, R. P. Johnson, T. J. Johnson, W. N. Johnson, T. Kamae, H. Katagiri, J. Kataoka, M. Kerr, J. Knödlseder, M. Kuss, J. Lande, S. Larsson, L. Latronico, C. Lavalley, M. Lemoine-Goumard, F. Longo, F. Loparco, B. Lott, M. N. Lovellette, P. Lubrano, M. N. Mazziotta, W. McConville, J. E. McEnery, J. Mehault, P. F. Michelson, W. Mitthumsiri, T. Mizuno, A. A. Moiseev, C. Monte, M. E. Monzani, A. Morselli, I. V. Moskalenko, S. Murgia, M. Naumann-Godo, R. Nemmen, S. Nishino, J. P. Norris, E. Nuss, M. Ohno, T. Ohsugi, A. Okumura, N. Omodei, M. Orienti, E. Orlando, J. F. Ormes, D. Paneque, J. H. Panetta, J. S. Perkins, M. Pesce-Rollins, M. Pierbattista, F. Piron, G. Pivato, T. A. Porter, J. L. Racusin, S. Rainò, R. Rando, M. Razzano, S. Razzaque, A. Reimer, O. Reimer, T. Reposeur, L. C. Reyes, S. Ritz, L. S. Rochester, C. Romoli, M. Roth, H. F.-W. Sadrozinski, D. A. Sanchez, P. M. Saz Parkinson, C. Sbarra, J. D. Scargle, C. Sgrò, J. Siegal-Gaskins, E. J. Siskind, G. Spandre, P. Spinelli, T. E. Stephens, D. J. Suson, H. Tajima, H. Takahashi, T. Tanaka, J. G. Thayer, J. B. Thayer, D. J. Thompson, L. Tibaldo, M. Tinivella, G. Tosti, E. Troja, T. L. Usher, J. Vandenbroucke, B. Van Klaveren, V. Vasileiou, G. Vianello, V. Vitale, A. P. Waite, E. Wallace, B. L. Winer, D. L. Wood, K. S. Wood, M. Wood, Z. Yang, S. Zimmer, The *FERMI* Large Area Telescope on orbit: Event classification, instrument response functions, and calibration. *Astrophys. J. Suppl. Ser.* **203**, 4 (2012). doi:10.1088/0067-0049/203/1/4

70. R. J. Gould, G. P. Schréder, Pair Production in Photon-Photon Collisions. *Phys. Rev.* **155**, 1404–1407 (1967). doi:10.1103/PhysRev.155.1404

71. F. W. Stecker, *Cosmic Gamma Rays* (NASA, 1971); https://ntrs.nasa.gov/archive/nasa/casi.ntrs.nasa.gov/19710015288.pdf.

72. R. W. Brown, K. O. Mikaelian, R. J. Gould, Absorption of High-Energy Cosmic Photons through Double-Pair Production in Photon-Photon Collisions. *Astrophys. Lett.* **14**, 203 (1973).

73. S. Cole, P. Norberg, C. M. Baugh, C. S. Frenk, J. Bland-Hawthorn, T. Bridges, R. Cannon, M. Colless, C. Collins, W. Couch, N. Cross, G. Dalton, R. De Propris, S. P. Driver, G. Efstathiou, R. S. Ellis, K. Glazebrook, C. Jackson, O. Lahav, I. Lewis, S. Lumsden, S. Maddox, D. Madgwick, J. A. Peacock, B. A. Peterson, W. Sutherland, K. Taylor, The 2dF galaxy redshift survey: Near-infrared galaxy luminosity functions. *Mon. Not. R. Astron. Soc.* **326**, 255–273 (2001). doi:10.1046/j.1365-8711.2001.04591.x

74. D. Foreman-Mackey, D. W. Hogg, D. Lang, J. Goodman, emcee: The MCMC Hammer. *Pub. Astron. Soc. Pac.* **125**, 306–312 (2013). doi:10.1086/670067

75. J. Goodman, J. Weare, Ensemble samplers with affine invariance. *Comm. App. Math. Comp. Sci.* **5**, 65–80 (2010). doi:10.2140/camcos.2010.5.65

76. F. W. Stecker, S. T. Scully, M. A. Malkan, An empirical determination of the intergalactic background light from UV to FIR wavelengths using FIR deep galaxy surveys and the gamma-ray opacity of the universe. *Astrophys. J.* **827**, 6 (2016). doi:10.3847/0004-637X/827/1/6

77. S. K. Andrews, S. P. Driver, L. J. M. Davies, C. P. Lagos, A. S. G. Robotham, Modelling the cosmic spectral energy distribution and extragalactic background light over all time. *Mon. Not. R. Astron. Soc.* **474**, 898–916 (2018). doi:10.1093/mnras/stx2843

78. V. Khaire, R. Srianand, Star formation history, dust attenuation, and extragalactic background light. *Astrophys. J.* **805**, 33 (2015). doi:10.1088/0004-637X/805/1/33

79. E. L. Wright, E. D. Reese, Detection of the Cosmic Infrared Background at 2.2 and 3.5 Microns Using DIRBE Observations. *Astrophys. J.* **545**, 43–55 (2000). doi:10.1086/317776

80. T. Matsumoto, S. Matsuura, H. Murakami, M. Tanaka, M. Freund, M. Lim, M. Cohen, M. Kawada, M. Noda, Infrared Telescope in Space Observations of the Near-Infrared Extragalactic Background Light. *Astrophys. J.* **626**, 31–43 (2005). doi:10.1086/429383

81. F. Aharonian, A. G. Akhperjanian, A. R. Bazer-Bachi, M. Beilicke, W. Benbow, D. Berge, K. Bernlöhr, C. Boisson, O. Bolz, V. Borrel, I. Braun, F. Breitling, A. M. Brown, P. M. Chadwick, L.-M. Chounet, R. Cornils, L. Costamante, B. Degrange, H. J. Dickinson, A. Djannati-Ataï, L. O. C. Drury, G. Dubus, D. Emmanoulopoulos, P. Espigat, F. Feinstein, G. Fontaine, Y. Fuchs, S. Funk, Y. A. Gallant, B. Giebels, S. Gillessen, J. F. Glicenstein, P. Goret, C. Hadjichristidis, D. Hauser, M. Hauser, G. Heinzelmann, G. Henri, G. Hermann, J. A. Hinton, W. Hofmann, M. Holleran, D. Horns, A. Jacholkowska, O. C. de

Jager, B. Khélifi, S. Klages, N. Komin, A. Konopelko, I. J. Latham, R. Le Gallou, A. Lemière, M. Lemoine-Goumard, N. Leroy, T. Lohse, J. M. Martin, O. Martineau-Huynh, A. Marcowith, C. Masterson, T. J. L. McComb, M. de Naurois, S. J. Nolan, A. Noutsos, K. J. Orford, J. L. Osborne, M. Ouchrif, M. Panter, G. Pelletier, S. Pita, G. Pühlhofer, M. Punch, B. C. Raubenheimer, M. Raue, J. Raux, S. M. Rayner, A. Reimer, O. Reimer, J. Ripken, L. Rob, L. Rolland, G. Rowell, V. Sahakian, L. Saugé, S. Schlenker, R. Schlickeiser, C. Schuster, U. Schwanke, M. Siewert, H. Sol, D. Spangler, R. Steenkamp, C. Stegmann, J.-P. Tavernet, R. Terrier, C. G. Théoret, M. Tluczykont, C. van Eldik, G. Vasileiadis, C. Venter, P. Vincent, H. J. Völk, S. J. Wagner, A low level of extragalactic background light as revealed by γ-rays from blazars. *Nature* **440**, 1018–1021 (2006). doi:10.1038/nature04680 Medline

82. MAGIC Collaboration, J. Albert, E. Aliu, H. Anderhub, L. A. Antonelli, P. Antoranz, M. Backes, C. Baixeras, J. A. Barrio, H. Bartko, D. Bastieri, J. K. Becker, W. Bednarek, K. Berger, E. Bernardini, C. Bigongiari, A. Biland, R. K. Bock, G. Bonnoli, P. Bordas, V. Bosch-Ramon, T. Bretz, I. Britvitch, M. Camara, E. Carmona, A. Chilingarian, S. Commichau, J. L. Contreras, J. Cortina, M. T. Costado, S. Covino, V. Curtef, F. Dazzi, A. De Angelis, E. De Cea Del Pozo, R. de Los Reyes, B. De Lotto, M. De Maria, F. De Sabata, C. D. Mendez, A. Dominguez, D. Dorner, M. Doro, M. Errando, M. Fagiolini, D. Ferenc, E. Fernández, R. Firpo, M. V. Fonseca, L. Font, N. Galante, R. J. G. López, M. Garczarczyk, M. Gaug, F. Goebel, M. Hayashida, A. Herrero, D. Höhne, J. Hose, C. C. Hsu, S. Huber, T. Jogler, T. M. Kneiske, D. Kranich, A. La Barbera, A. Laille, E. Leonardo, E. Lindfors, S. Lombardi, F. Longo, M. López, E. Lorenz, P. Majumdar, G. Maneva, N. Mankuzhiyil, K. Mannheim, L. Maraschi, M. Mariotti, M. Martínez, D. Mazin, M. Meucci, M. Meyer, J. M. Miranda, R. Mirzoyan, S. Mizobuchi, M. Moles, A. Moralejo, D. Nieto, K. Nilsson, J. Ninkovic, N. Otte, I. Oya, M. Panniello, R. Paoletti, J. M. Paredes, M. Pasanen, D. Pascoli, F. Pauss, R. G. Pegna, M. A. Perez-Torres, M. Persic, L. Peruzzo, A. Piccioli, F. Prada, E. Prandini, N. Puchades, A. Raymers, W. Rhode, M. Ribó, J. Rico, M. Rissi, A. Robert, S. Rügamer, A. Saggion, T. Y. Saito, M. Salvati, M. Sanchez-Conde, P. Sartori, K. Satalecka, V. Scalzotto, V. Scapin, R. Schmitt, T. Schweizer, M. Shayduk, K. Shinozaki, S. N. Shore, N. Sidro, A. Sierpowska-Bartosik, A. Sillanpää, D. Sobczynska, F. Spanier, A. Stamerra, L. S. Stark, L. Takalo, F. Tavecchio, P. Temnikov, D. Tescaro, M. Teshima, M. Tluczykont, D. F. Torres, N. Turini, H. Vankov, A. Venturini, V. Vitale, R. M. Wagner, W. Wittek, V. Zabalza, F. Zandanel, R. Zanin, J. Zapatero, Very-high-energy gamma rays from a distant quasar: How transparent is the universe? *Science* **320**, 1752–1754 (2008). doi:10.1126/science.1157087 Medline

83. A. Domínguez, M. Ajello, Spectral analysis of *FERMI*-LAT blazars above 50 GeV. *Astrophys. J.* **813**, L34 (2015). doi:10.1088/2041-8205/813/2/L34

84. T. Armstrong, A. M. Brown, P. M. Chadwick, Fermi-LAT high-z active galactic nuclei and the extragalactic background light. *Mon. Not. R. Astron. Soc.* **470**, 4089–4098 (2017). doi:10.1093/mnras/stx1309

85. M. L. Ahnen, S. Ansoldi, L. A. Antonelli, P. Antoranz, A. Babic, B. Banerjee, P. Bangale, U. B. Almeida, J. A. Barrio, W. Bednarek, E. Bernardini, B. Biasuzzi, A. Biland, O. Blanch, S. Bonnefoy, G. Bonnoli, F. Borracci, T. Bretz, E. Carmona, A. Carosi, A. Chatterjee, R. Clavero, P. Colin, E. Colombo, J. L. Contreras, J. Cortina, S. Covino, P. D. Vela, F. Dazzi, A. D. Angelis, B. D. Lotto, E. O. Wilhelmi, C. D. Mendez, F. D. Pierro, D. D. Prester, D. Dorner, M. Doro, S. Einecke, D. E. Glawion, D. Elsaesser, A. Fernández-Barral, D. Fidalgo, M. V. Fonseca, L. Font, K. Frantzen, C. Fruck, D. Galindo, R. J. G. López, M. Garczarczyk, D. G. Terrats, M. Gaug, P. Giammaria, N. Godinović, A. G. Muñoz, D. Guberman, A. Hahn, Y. Hanabata, M. Hayashida, J. Herrera, J. Hose, D. Hrupec, G. Hughes, W. Idec, K. Kodani, Y. Konno, H. Kubo, J. Kushida, A. L. Barbera, D. Lelas, E. Lindfors, S. Lombardi, M. López, R. López-Coto, A. López-Oramas, E. Lorenz, P. Majumdar, M. Makariev, K. Mallot, G. Maneva, M. Manganaro, K. Mannheim, L. Maraschi, B. Marcote, M. Mariotti, M. Martínez, D. Mazin, U. Menzel, J. M. Miranda, R. Mirzoyan, A. Moralejo, E. Moretti, D. Nakajima, V. Neustroev, A. Niedzwiecki, M. N. Rosillo, K. Nilsson, K. Nishijima, K. Noda, R. Orito, A. Overkemping, S. Paiano, J. Palacio, M. Palatiello, D. Paneque, R. Paoletti, J. M. Paredes, X. Paredes-Fortuny, M. Persic, J. Poutanen, P. G. P. Moroni, E. Prandini, I. Puljak, W. Rhode, M. Ribó, J. Rico, J. R. Garcia, T. Saito, K. Satalecka, C. Schultz, T. Schweizer, S. N. Shore, A. Sillanpää, J. Sitarek, I. Snidaric, D. Sobczynska, A. Stamerra, T. Steinbring, M. Strzys, L. Takalo, H. Takami, F. Tavecchio, P. Temnikov, T. Terzić, D. Tescaro, M. Teshima, J. Thaele, D. F. Torres, T. Toyama, A. Treves, V. Verguilov, I. Vovk, J. E. Ward, M. Will, M. H. Wu, R. Zanin, M. Ajello, L. Baldini, G. Barbiellini, D. Bastieri, J. B. González, R. Bellazzini, E. Bissaldi, R. D. Blandford, R. Bonino, J. Bregeon, P. Bruel, S. Buson, G. A. Caliandro, R. A. Cameron, M. Caragiulo, P. A. Caraveo, E. Cavazzuti, J. Chiang, G. Chiaro, S. Ciprini, F. D'Ammando, F. Palma, R. Desiante, L. D. Venere, A. Domínguez, P. Fusco, F. Gargano, D. Gasparrini, N. Giglietto, F. Giordano, M. Giroletti, I. A. Grenier, S. Guiriec, E. Hays, J. W. Hewitt, T. Jogler, M. Kuss, S. Larsson, J. Li, L. Li, F. Longo, F. Loparco, M. N. Lovellette, P. Lubrano, S. Maldera, M. Mayer, M. N. Mazziotta, J. E. McEnery, N. Mirabal, T. Mizuno, M. E. Monzani, A. Morselli, I. V. Moskalenko, E. Nuss, R. Ojha, T. Ohsugi, N. Omodei, E. Orlando, J. S. Perkins, M. Pesce-Rollins, F. Piron, G. Pivato, T. A. Porter, S. Raino, R. Rando, M. Razzano, A. Reimer, O. Reimer, C. Sgro, E. J. Siskind, F. Spada, G. Spandre, P. Spinelli, H. Tajima, H. Takahashi, J. B. Thayer, D. J. Thompson, E. Troja, K. S. Wood, M. Balokovic, A. Berdyugin, A. Carraminana, L. Carrasco, V. Chavushyan, V. F. Ramazani, M. Feige, S. Haarto, P. Haeusner, T. Hovatta, J. Kania, J. Klamt, A. Lähteenmäki, J. Leon-Tavares, C. Lorey, L. Pacciani, A. Porras, E. Recillas, R. Reinthal, M. Tornikoski, D. Wolfert, N. Zottmann, Very high energy γ -rays from the universe's middle age: Detection of the z =

0.940 blazar PKS 1441+25 with MAGIC. *Astrophys. J.* **815**, L23 (2015). doi:10.1088/2041-8205/815/2/L23

86. M. L. Ahnen, S. Ansoldi, L. A. Antonelli, P. Antoranz, C. Arcaro, A. Babic, B. Banerjee, P. Bangale, U. Barres de Almeida, J. A. Barrio, J. Becerra González, W. Bednarek, E. Bernardini, A. Berti, B. Biasuzzi, A. Biland, O. Blanch, S. Bonnefoy, G. Bonnoli, F. Borracci, T. Bretz, S. Buson, A. Carosi, A. Chatterjee, R. Clavero, P. Colin, E. Colombo, J. L. Contreras, J. Cortina, S. Covino, P. De Vela, F. Dazzi, A. De Angelis, B. De Lotto, E. de Oña Wilhelmi, F. Di Pierro, M. Doert, A. Domínguez, D. Dominis Prester, D. Dorner, M. Doro, S. Einecke, D. Eisenacher Glawion, D. Elsaesser, M. Engelkemeier, V. Fallah Ramazani, A. Fernández-Barral, D. Fidalgo, M. V. Fonseca, L. Font, K. Frantzen, C. Fruck, D. Galindo, R. J. García López, M. Garczarczyk, D. Garrido Terrats, M. Gaug, P. Giammaria, N. Godinović, D. Gora, D. Guberman, D. Hadasch, A. Hahn, M. Hayashida, J. Herrera, J. Hose, D. Hrupec, G. Hughes, W. Idec, K. Kodani, Y. Konno, H. Kubo, J. Kushida, A. La Barbera, D. Lelas, E. Lindfors, S. Lombardi, F. Longo, M. López, R. López-Coto, P. Majumdar, M. Makariev, K. Mallot, G. Maneva, M. Manganaro, K. Mannheim, L. Maraschi, B. Marcote, M. Mariotti, M. Martínez, D. Mazin, U. Menzel, J. M. Miranda, R. Mirzoyan, A. Moralejo, E. Moretti, D. Nakajima, V. Neustroev, A. Niedzwiecki, M. Nievas Rosillo, K. Nilsson, K. Nishijima, K. Noda, L. Nogués, S. Paiano, J. Palacio, M. Palatiello, D. Paneque, R. Paoletti, J. M. Paredes, X. Paredes-Fortuny, G. Pedaletti, M. Peresano, L. Perri, M. Persic, J. Poutanen, P. G. Prada Moroni, E. Prandini, I. Puljak, J. R. Garcia, I. Reichardt, W. Rhode, M. Ribó, J. Rico, T. Saito, K. Satalecka, S. Schroeder, T. Schweizer, S. N. Shore, A. Sillanpää, J. Sitarek, I. Snidaric, D. Sobczynska, A. Stamerra, M. Strzys, T. Surić, L. Takalo, F. Tavecchio, P. Temnikov, T. Terzić, D. Tescaro, M. Teshima, D. F. Torres, T. Toyama, A. Treves, V. Verguilov, I. Vovk, J. E. Ward, M. Will, M. H. Wu, R. Zanin, R. Desiante, Detection of very high energy gamma-ray emission from the gravitationally lensed blazar QSO B0218+357 with the MAGIC telescopes. *Astron. Astrophys.* **595**, A98 (2016). doi:10.1051/0004-6361/201629461

87. P. Madau, in *After the Dark Ages: When Galaxies Were Young (The Universe at 2 < Z < 5)*, S. Holt, E. Smith, Eds. (American Institute of Physics, 1999), pp. 299–311.

88. S. L. Finkelstein, C. Papovich, R. E. Ryan, A. H. Pawlik, M. Dickinson, H. C. Ferguson, K. Finlator, A. M. Koekemoer, M. Giavalisco, A. Cooray, J. S. Dunlop, S. M. Faber, N. A. Grogin, D. D. Kocevski, J. A. Newman, CANDELS: The contribution of the observed galaxy population to cosmic reionization. *Astrophys. J.* **758**, 93 (2012). doi:10.1088/0004-637X/758/2/93

89. A. Kashlinsky, Cosmic Infrared Background from Population III Stars and Its Effect on Spectra of High- *z* Gamma-Ray Bursts. *Astrophys. J.* **633**, L5–L8 (2005). doi:10.1086/498243

90. R. J. Bouwens, G. D. Illingworth, P. A. Oesch, I. Labbé, P. G. van Dokkum, M. Trenti, M. Franx, R. Smit, V. Gonzalez, D. Magee, UV-continuum slopes of >4000 $z \sim$ 4-8 galaxies from the HUDF/XDF, HUDF09, ERS, CANDELS-South, and CANDELS-North fields. *Astrophys. J.* **793**, 115 (2014). doi:10.1088/0004-637X/793/2/115

91. R. S. Ellis, R. J. McLure, J. S. Dunlop, B. E. Robertson, Y. Ono, M. A. Schenker, A. Koekemoer, R. A. A. Bowler, M. Ouchi, A. B. Rogers, E. Curtis-Lake, E. Schneider, S. Charlot, D. P. Stark, S. R. Furlanetto, M. Cirasuolo, The abundance of star-forming galaxies in the redshift range 8.5-12: New results from the 2012 Hubble ultra deep field campaign. *Astrophys. J.* **763**, L7 (2013). doi:10.1088/2041-8205/763/1/L7

92. G. Chabrier, Galactic Stellar and Substellar Initial Mass Function. *Publ. Astron. Soc. Pac.* **115**, 763–795 (2003). doi:10.1086/376392

93. E. E. Salpeter, The Luminosity Function and Stellar Evolution. *Astrophys. J.* **121**, 161 (1955). doi:10.1086/145971

94. R. J. Bouwens, M. Aravena, R. Decarli, F. Walter, E. da Cunha, I. Labbé, F. E. Bauer, F. Bertoldi, C. Carilli, S. Chapman, E. Daddi, J. Hodge, R. J. Ivison, A. Karim, O. Le Fevre, B. Magnelli, K. Ota, D. Riechers, I. R. Smail, P. van der Werf, A. Weiss, P. Cox, D. Elbaz, J. Gonzalez-Lopez, L. Infante, P. Oesch, J. Wagg, S. Wilkins, ALMA spectroscopic survey in the Hubble ultra deep field: The infrared excess of UV-selected z = 2–10 galaxies as a function of UV-continuum slope and stellar mass. *Astrophys. J.* **833**, 72 (2016). doi:10.3847/1538-4357/833/1/72

95. O. Cucciati, L. Tresse, O. Ilbert, O. Le Fèvre, B. Garilli, V. Le Brun, P. Cassata, P. Franzetti, D. Maccagni, M. Scodeggio, E. Zucca, G. Zamorani, S. Bardelli, M. Bolzonella, R. M. Bielby, H. J. McCracken, A. Zanichelli, D. Vergani, The star formation rate density and dust attenuation evolution over 12 Gyr with the VVDS surveys. *Astron. Astrophys.* **539**, A31 (2012). doi:10.1051/0004-6361/201118010

96. T. T. Takeuchi, V. Buat, D. Burgarella, The evolution of the ultraviolet and infrared luminosity densities in the universe at $0 < z < 1$. *Astron. Astrophys.* **440**, L17–L20 (2005). doi:10.1051/0004-6361:200500158

97. N. A. Reddy, C. C. Steidel, A steep faint-end slope of the UV luminosity function at $z \sim$ 2-3: Implications for the global stellar mass density and star formation in low-mass halos. *Astrophys. J.* **692**, 778–803 (2009). doi:10.1088/0004-637X/692/1/778

98. T. K. Wyder, M. A. Treyer, B. Milliard, D. Schiminovich, S. Arnouts, T. Budavári, T. A. Barlow, L. Bianchi, Y.-I. Byun, J. Donas, K. Forster, P. G. Friedman, T. M. Heckman, P. N. Jelinsky, Y.-W. Lee, B. F. Madore, R. F. Malina, D. C. Martin, P. Morrissey, S. G. Neff, R. M. Rich, O. H. W. Siegmund, T. Small, A. S. Szalay, B. Y. Welsh, The Ultraviolet Galaxy Luminosity Function in the Local Universe from *GALEX* Data. *Astrophys. J.* **619**, L15–L18 (2005). doi:10.1086/424735

99. A. S. G. Robotham, S. P. Driver, The GALEX-SDSS NUV and FUV flux density and local star formation rate. *Mon. Not. R. Astron. Soc.* **413**, 2570–2582 (2011). doi:10.1111/j.1365-2966.2011.18327.x

100. T. Dahlen, B. Mobasher, M. Dickinson, H. C. Ferguson, M. Giavalisco, C. Kretchmer, S. Ravindranath, Evolution of the Luminosity Function, Star Formation Rate, Morphology, and Size of Star-forming Galaxies Selected at Rest-Frame 1500 and 2800 A. *Astrophys. J.* **654**, 172–185 (2007). doi:10.1086/508854

101. M. Yoshida, K. Shimasaku, N. Kashikawa, M. Ouchi, S. Okamura, M. Ajiki, M. Akiyama, H. Ando, K. Aoki, M. Doi, H. Furusawa, T. Hayashino, F. Iwamuro, M. Iye, H. Karoji, N. Kobayashi, K. Kodaira, T. Kodama, Y. Komiyama, M. A. Malkan, Y. Matsuda, S. Miyazaki, Y. Mizumoto, T. Morokuma, K. Motohara, T. Murayama, T. Nagao, K. Nariai, K. Ohta, T. Sasaki, Y. Sato, K. Sekiguchi, Y. Shioya, H. Tamura, Y. Taniguchi, M. Umemura, T. Yamada, N. Yasuda, Luminosity Functions of Lyman Break Galaxies at z~4 and z~5 in the Subaru Deep Field. *Astrophys. J.* **653**, 988–1003 (2006). doi:10.1086/508621

102. L. Tresse, O. Ilbert, E. Zucca, G. Zamorani, S. Bardelli, S. Arnouts, S. Paltani, L. Pozzetti, D. Bottini, B. Garilli, V. Le Brun, O. Le Fèvre, D. Maccagni, J.-P. Picat, R. Scaramella, M. Scodeggio, G. Vettolani, A. Zanichelli, C. Adami, M. Arnaboldi, M. Bolzonella, A. Cappi, S. Charlot, P. Ciliegi, T. Contini, S. Foucaud, P. Franzetti, I. Gavignaud, L. Guzzo, A. Iovino, H. J. McCracken, B. Marano, C. Marinoni, A. Mazure, B. Meneux, R. Merighi, R. Pellò, A. Pollo, M. Radovich, M. Bondi, A. Bongiorno, G. Busarello, O. Cucciati, F. Lamareille, G. Mathez, Y. Mellier, P. Merluzzi, V. Ripepi, The cosmic star formation rate evolution from $z = 5$ to $z = 0$ from the VIMOS VLT deep survey. *Astron. Astrophys.* **472**, 403–419 (2007). doi:10.1051/0004-6361:20066330

103. M. Raue, M. Meyer, Probing the peak of the star formation rate density with the extragalactic background light. *Mon. Not. R. Astron. Soc.* **426**, 1097 (2012). doi:10.1111/j.1365-2966.2012.21744.x

104. N. Bourne, J. S. Dunlop, E. Merlin, S. Parsa, C. Schreiber, M. Castellano, C. J. Conselice, K. E. K. Coppin, D. Farrah, A. Fontana, J. E. Geach, M. Halpern, K. K. Knudsen, M. J. Michalowski, A. Mortlock, P. Santini, D. Scott, X. W. Shu, C. Simpson, J. M. Simpson, D. J. B. Smith, P. P. van der Werf, Evolution of cosmic star formation in the SCUBA-2 Cosmology Legacy Survey. *Mon. Not. R. Astron. Soc.* **467**, 1360 (2017). doi:10.1093/mnras/stx031

105. M. D. Kistler, H. Yüksel, J. F. Beacom, A. M. Hopkins, J. S. B. Wyithe, The star formation rate in the reionization era as indicated by gamma-ray bursts. *Astrophys. J.* **705**, L104–L108 (2009). doi:10.1088/0004-637X/705/2/L104

106. S. P. Driver, S. K. Andrews, E. da Cunha, L. J. Davies, C. Lagos, A. S. G. Robotham, K. Vinsen, A. H. Wright, M. Alpaslan, J. Bland-Hawthorn, N. Bourne, S. Brough, M. N.

Bremer, M. Cluver, M. Colless, C. J. Conselice, L. Dunne, S. A. Eales, H. Gomez, B. Holwerda, A. M. Hopkins, P. R. Kafle, L. S. Kelvin, J. Loveday, J. Liske, S. J. Maddox, S. Phillipps, K. Pimbblet, K. Rowlands, A. E. Sansom, E. Taylor, L. Wang, S. M. Wilkins, GAMA/G10-COSMOS/3D-HST: The $0 < z < 5$ cosmic star formation history, stellar-mass, and dust-mass densities. *Mon. Not. R. Astron. Soc.* **475**, 2891–2935 (2018). doi:10.1093/mnras/stx2728

107. R. J. Bouwens, G. D. Illingworth, P. A. Oesch, M. Trenti, I. Labbé, L. Bradley, M. Carollo, P. G. van Dokkum, V. Gonzalez, B. Holwerda, M. Franx, L. Spitler, R. Smit, D. Magee, UV luminosity functions at redshifts $z \sim 4$ to $z \sim 10$: 10,000 galaxies from *HST* legacy fields. *Astrophys. J.* **803**, 34 (2015). doi:10.1088/0004-637X/803/1/34

108. S. Razzaque, C. D. Dermer, J. D. Finke, The stellar contribution to the extragalactic background light and absorption of high-energy gamma rays. *Astrophys. J.* **697**, 483–492 (2009). doi:10.1088/0004-637X/697/1/483

109. P. P. Eggleton, M. J. Fitchett, C. A. Tout, The distribution of visual binaries with two bright components. *Astrophys. J.* **347**, 998 (1989). doi:10.1086/168190

110. S. P. Driver, C. C. Popescu, R. J. Tuffs, A. W. Graham, J. Liske, I. Baldry, The Energy Output of the Universe from 0.1 to 1000 μm. *Astrophys. J.* **678**, L101–L104 (2008). doi:10.1086/588582

111. Y. Gong, A. Cooray, The extragalactic background light from the measurements of the attenuation of high-energy gamma-ray spectrum. *Astrophys. J.* **772**, L12 (2013). doi:10.1088/2041-8205/772/1/L12

112. A. M. Hopkins, J. F. Beacom, On the Normalization of the Cosmic Star Formation History. *Astrophys. J.* **651**, 142–154 (2006). doi:10.1086/506610

113. P. Madau, F. Haardt, Cosmic reionization after Planck: Could quasars do it all? *Astrophys. J.* **813**, L8 (2015). doi:10.1088/2041-8205/813/1/L8

114. E. Lusso, G. Worseck, J. F. Hennawi, J. X. Prochaska, C. Vignali, J. Stern, J. M. O'Meara, The first ultraviolet quasar-stacked spectrum at $z \simeq 2.4$ from WFC3. *Mon. Not. R. Astron. Soc.* **449**, 4204–4220 (2015). doi:10.1093/mnras/stv516

115. V. Khaire, R. Srianand, New synthesis models of consistent extragalactic background light over cosmic time. arXiv:1801.09693 (29 January 2018).